CLIMATE RECONSTRUCTION USING TRACE ELEMENT AND STABLE ISOTOPE SIGNATURES PRESERVED IN AN EARLY LATE PLEISTOCENE STALAGMITE FROM BUCKEYE CREEK CAVE, APPALACHIAN MOUNTAINS, SOUTHERN WEST VIRGINIA, USA

by

ASHLEY RACHELLE WRIGHT

Presented to the Faculty of the Graduate School of
The University of Texas at Arlington in Partial Fulfillment
of the Requirements
for the Degree of

MASTER OF SCIENCE IN GEOLOGY

THE UNIVERSITY OF TEXAS AT ARLINGTON
DECEMBER 2011

ACKNOWLEDGEMENTS

I would like to thank my encouraging and brilliant family for all of their support and motivation. Thanks to my mother, Kathie Norris, for always believing I can do more and for being the common denominator. Thanks to my father, Trent Norris, for always being there and ignoring my tantrums. Thanks to my grandmother, Jean Harris, for keeping me on track to graduation. Thanks to my brother, Trevor Norris, for being my best friend and guiding light over the years. Thanks to Chance Norris and Tyler Fredrickson for being so intelligent that the competition motivated me to continue my education. Thanks to the love of my life, Billy Fisher, for the assistance, motivation and love you have shown me over the years of my education.

Many thanks to my committee: Dr. Harold Rowe, Dr. John Wickham, and Dr. Andrew Hunt. To my committee chair, Dr. Rowe, I cannot thank you enough for all of your guidance and motivation not only with my thesis, but also with taking advantage of the various opportunities to begin and advance my career. You are an amazing, brilliant, and compassionate professor, and I thank you for all that you have given me.

November 21, 2011

ABSTRACT

CLIMATE RECONSTRUCTION USING TRACE ELEMENT AND STABLE ISOTOPE SIGNATURES PRESERVED IN AN EARLY LATE PLEISTOCENE STALAGMITE FROM BUCKEYE CREEK CAVE, APPALACHIAN MOUNTAINS, SOUTHERN WEST VIRGINIA, USA

Ashley Rachelle Wright, M.S. Geology

The University of Texas at Arlington, 2011

Supervising Professor: Harold Rowe

An early-Late Pleistocene stalagmite was recovered from Buckeye Creek Cave (37°58.57'N, 80°23.98'W), southeastern West Virginia, USA. The growth axis of stalagmite BCC-025 was sampled for $\delta^{18}O$, $\delta^{13}C$, and Sr/Ca of the calcite. A crude age model was developed using two Th-230 ages, from the top (~490 kyrBP) and bottom (~630 kyrBP) of the stalagmite. A more elaborate age model for stalagmite growth was developed using established marine isotope stage (MIS 13/14, 14/15, 15/16) boundaries. Overall, the MIS boundaries approximate the locations of major hiatuses along the axis of stalagmite growth. The proxy records developed from BCC-025 reveal less covariation and overall diminished absolute ranges when compared to younger records, potentially, because the glacial/interglacial variability of the early-Late Pleistocene is less than that of the Late Pleistocene. Despite the need for better age constraints, the observations and interpretations provide an initial window into the drivers and extent of climate change before the more pronounced swings of glacial/interglacial variability of the Late Pleistocene.

TABLE OF CONTENTS

LIST OF ILLUSTRATIONS

LIST OF TABLES

CHAPTER 1

INTRODUCTION

1.1 Research Objectives

The primary purpose of the present research is to demonstrate that past climate changes can be inferred by evaluating the stable isotopic and geochemical records preserved along the growth axes of stalagmite samples from Buckeye Creek Cave, Appalachian Mountains, southwestern West Virginia. Studying past climate changes and integrating paleoclimate records is complicated by the variable temporal resolution of different records and the immense spatial scales involved. Throughout this study, several questions were presented and evaluated:

1) What were the timing, magnitude, and duration of climate changes in the study region during the period from ~490 to ~630 thousand years before present (kyrBP)?
2) What were the underlying mechanisms responsible for climate change and seasonality of the region?
3) What environmental conditions can be inferred from the record?
4) Can the suite of analyses and subsequent interpretation provide sufficient foundation to establish an understanding of mid-latitude climate in the middle to late Pleistocene?

Ultimately, the study attempts to provide a more complete understanding of (1) past climate change in the south-central Appalachian region of eastern North America, and (2) how regional climate change is associated with the previously documented, global climate shifts inferred from other paleoarchives.

The remainder of the introduction focuses on (1) developing an understanding of how calcitic cave stalagmites are utilized to reconstruct climate and environmental change, and (2)

demonstrating the importance of understanding and integrating existing global climate records that will ultimately aid in the interpretation and temporal relation of the stalagmite record produced in the present study.

1.2 Stalagmites as Climate Archives

Stalagmites are cave formations that grow upward from the floor due to drip-water deposition from above (Figure 1.1). Stalagmites take on a variety of forms, from tall, spindly broomsticks to complex, multi-tiered towers. Cylindrically shaped stalagmites are favored for paleoclimate study due to their relatively simple (often layer-cake) growth geometry. Stalagmite shape and diameter are determined largely by drip rate (narrower for low flows), ceiling height (diameter increases with fall height), cave atmosphere conditions, and the carbonate chemistry of the drip-water solution (more supersaturated waters may tend to precipitate more irregularly) (Kaufmann and Dreybrodt, 2004; Fairchild et al., 2006). Stalagmites can grow semi-continuously for many thousands of years, all the while encoding climatic information from the time of their deposition in both their geometry and geochemistry. Presumably, they capture the cave response to the external environment, which is partially controlled by the distribution, quantity, and chemistry of the water infiltrating through the overlying karstic aquifer, showing minute secondary alteration (Fairchild et al., 2006).

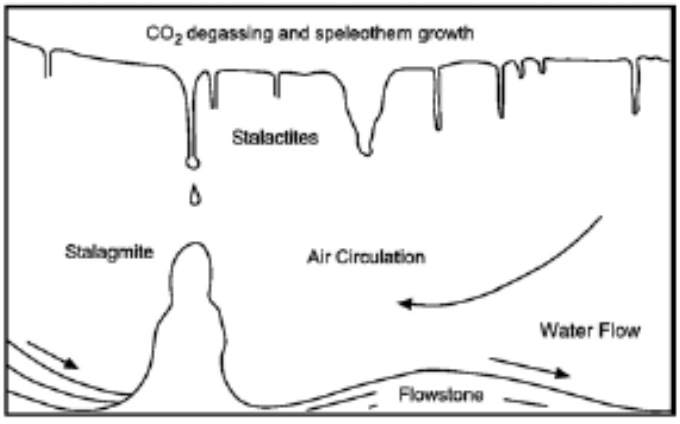

Figure 1.1 Schematic representation of speleothem formation and habitation within the cave environment (Fairchild et al., 2006).

Cave climate is influenced by the cave geometry, overlying hydrological properties, and external climate (Fairchild et al., 2007). Two parameters of the cave environment enable the use of stalagmites in reconstructing past climate: cave temperatures and humidity (McDermott, 2004). Cave air temperatures, which remain relatively constant throughout the year (typically ± 1°C), are approximately equal to the above-cave mean annual temperature. Cave air, in cool temperate regions, is characterized by very high humidity levels (typically 95-99%); which minimizes evaporation that might promote kinetic isotope fractionation, increasing the complexity of past climate interpretation (McDermott, 2004). Stalagmite deposition typically occurs by the degassing of CO_2 from the carbonate saturated drip-waters when entering the cave atmosphere, not by the evaporation of water (Dorale et al., 1998). Stalagmite calcite deposition occurs after water infiltrates through the soil overlying a cave, where elevated carbon dioxide concentrations are produced in the soil atmosphere as microbes decompose organic matter (derived from vegetation) and as plant roots respire. The carbon dioxide dissolves limestone ($CaCO_3$) to form calcium bicarbonate ($Ca(HCO_3)_2$), in the ground water. Figure 1.2 illustrates the dissolution and precipitation scheme in the soil zone, epikarst zone, and into the cave atmosphere that facilitate speleothem formation. Soil water movement, storage, and evaporation are controlled by the surface climate and the soil physical properties (Shurbaji and Phillips, 1995). Karst aquifers display complex flow phenomena because the porosity occurs in three forms: as conduits, fractures, and pervasive matrix. The epikarst functions as a perched aquifer which feeds both major conduits, and lower transmissivity fissures. In turn, the conduits and fissures tend to feed zones of drip-water in caves, reflecting the amount of infiltration (Fairchild et al., 2006). As the groundwater flows into the cave (which has lower CO_2 concentration), CO_2 is given off into the cave atmosphere. The release of CO_2 reverses the reaction to where calcite ($CaCO_3$) is then deposited within the cave, as a stalagmite (Wilson, 1980). Drip-water degassing is driven by the difference between the pCO_2 of the water in the epikarst and of that in the cave air.

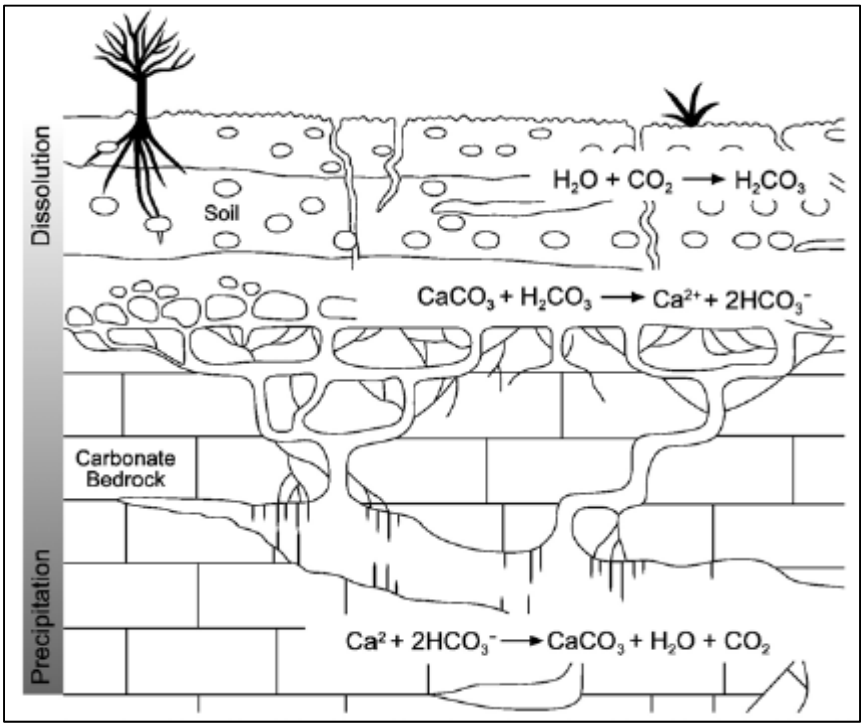

Figure 1.2 Illustration of dissolution and precipitation scheme within the karstic system (Fairchild et al., 2006).

Stalagmite isotopic and geochemical compositions are directly associated with the chemistry of drip-water which is linked to the chemistry of the overlying soil and isotopic composition of precipitation (Houghton et al., 2001).

Stalagmite growth rates vary depending on factors such as temperature and calcium ion concentration of the drip-waters. Slow deposition of stalagmites can drastically reduce the resolution of the isotope signal, which results in the loss of detection of significant, but short-lived events such as the 8.2 kyr cooling event (McDermott 2004). Extreme climatic conditions like glaciations and flooding can reduce or cease the growth of stalagmites, such as the case of the Villars Cave stalagmite growth patterns (Genty et al., 2003). Growth of the Villars Cave stalagmite, southwest France, was suspended for about 6000 years during the last glacial period (~55.7-81.8 kyrBP) due to extreme cold temperatures. Similarly, Panno et al. (2004)

observed cessation of stalagmite growth due to flooding of the Fogelpole Cave in Illinois. Global glacial events, which cause reduced precipitation and regional changes to carbon cycles, which are induced by events such as El Niño (causing increased precipitation) can also be resolved from stalagmites (Frappier et al., 2002).

Three important variables influencing stalagmite growth are location with respect to cave entrances, depth below the surface, and position with respect to the flow-line of water within the cave (Fairchild et al., 2006). In carefully chosen sites, stalagmites can record key aspects of climate variability such as mean annual temperature, rainfall variability, atmospheric circulation changes and vegetation response in a variety of measurable parameters, such as stable isotope ratios, inter-annual thickness variations of growth laminae, growth-rate changes, variations in trace element ratios, organic acid contents, and the nature of trapped pollen grains (McDermott, 2004). Interpretation of the various proxies preserved in stalagmites is difficult in terms of simple climate variables (i.e., temperature) because of the various possible influences on speleothem growth, geochemistry and morphology, such as the source temperature, rainfall seasonality, groundwater residence time, soil/vegetation, aquifer development, and primary speleothem crystal growth (Jones and Mann, 2004; Fairchild et al., 2006).

1.3 Speleothem Geochemistry

Speleothems, the generic term given for all cave formations such as stalagmites, stalactites, and flowstones (Hill and Forti, 1997), are valuable multi-proxy archives of past terrestrial climatic conditions because: (1) They grow continuously over thousands of years in sheltered cave environments; (2) They allow precise dating using the U/Th-method (Richards and Dorale, 2003; Scholtz and Hoffman, 2008); (3) They offer several proxies that can be measured at high-resolution (Musgrove et al., 2001; Wackerbath et al., 2010); (4) Finally, speleothems are located globally, including low-altitude, low-latitude terrestrial environments where other high-resolution climate records may be scarce (Mickler et al., 2004; Mickler et al., 2006). Stable isotope signatures and trace element ratios preserved along the growth-axes of

speleothems are often used to generate the most fundamental proxy records of past climate change (Fairchild and Treble 2009), and are often interpreted to infer changes in paleoprecipitation, paleotemperature, and paleovegetation (Dorale et al., 1992; Winograd et al., 1992; Baker et al., 1998; Genty et al., 1998). Other speleothem proxies for environmental change are growth rate, organic matter content, stratigraphic columns, and luminescent laminae (McDermott et al., 1999; Lauritzen, 2003). These proxy-based reconstructions of past climate have placed recent large-scale warming in an appropriate long-term, big-picture context (Jones and Mann, 2004). Fairchild et al. (2006) distinguish five sources of variation that influence speleothem geochemistry, where the direct role of climate diminishes progressively, 1) atmospheric, 2) vegetation/soil, 3) karstic aquifer, 4) primary speleothem crystal growth, and 5) secondary alteration. Speleothem records can provide pertinent information regarding changes in the hydrological cycle, linking to the understanding of atmospheric circulation, which strengthens interpretations of climate.

1.3.1. $\delta^{18}O$ of Stalagmite Calcite

The oxygen isotopic signature ($\delta^{18}O$) preserved in stalagmite calcite is linked to the meteoric water – a hydrologic term for surface and ground water that originated in the atmosphere as rain or condensation reaching the zone of saturation by infiltration – and used to estimate relative changes in mean annual temperature during stalagmite growth (Hendy, 1971; Dorale et al., 1998, Denniston et al., 2007). The $\delta^{18}O$ of cave drip-water should record the ^{18}O:^{16}O ratio of the meteoric water that falls on the surface above the cave (Palmer, 2002). Therefore, the $\delta^{18}O$ values of stalagmites can be used, in correlation with other proxies to reconstruct ancient temperature and moisture sources. Stalagmite calcite $\delta^{18}O$ signatures are interpreted as variations in cave temperature and properties of rainfall (temperature, air mass trajectory, source, and amount effects) (McDermott et al., 2004). For the modern mid-latitudes, the $\delta^{18}O$ value of mean annual precipitation (MAP) in continental interiors is observed to be primarily a function of the mean annual atmospheric temperature (MAT). The modern empirical

relationship between MAP $\delta^{18}O$ values and MAT is ~0.6 ‰/°C (Dansgaard, 1964; Friedman et al., 1977; Gat, 1983), thus speleothem calcite that grows in isotopic equilibrium with cave drip-waters under stable ambient conditions has traditionally been inferred to preserve the mean annual temperature (Moore and Sullivan, 1978). Assuming little to no kinetic effects, the equilibrium fractionation factor between calcite and water (-0.26 ‰/°C; O'Neil and Epstein, 1966) must still be considered when reconstructing past atmospheric temperatures. This isotopic offset must be included with the modern empirical relationship of ~0.6 ‰/°C, yielding an overall estimated linkage between MAP $\delta^{18}O$ values and MAT of ~0.35 ‰/°C (Dorale et al., 1998).

There are various effects (controls) on the $\delta^{18}O$ in precipitation that may obscure the relationship between MAP and MAT: (1) A temperature effect, where lower average temperatures cause increased depletion of ^{18}O in vapor masses, predominately in areas of high latitude with increased rainout (Dansgaard, 1964; Rozanski et al., 1992); (2) A continental effect, where the further inland a vapor mass is from its original oceanic source, the more depleted in ^{18}O it is, varying regionally, based on established storm paths (Ingraham, 1998); (3) An elevation effect, where regions of high elevation leave vapor masses increasingly depleted in ^{18}O due to the increased rainout and fractionation factors from the cooler temperatures at higher elevation (correlating with the temperature effect) (Friedman and Smith, 1970; Clark and Fritz, 1997); (4) Lastly, an amount effect, where precipitation is increasingly depleted in ^{18}O as monthly or mean annual precipitation increases (Dansgaard, 1964). This is mainly because $H_2{}^{18}O$ has a slightly lower vapor pressure than $H_2{}^{16}O$, lowering the cloud base and allowing continuous isotopic exchange with falling raindrops; as precipitation continues, the area beneath the vapor mass is increasingly depleted in ^{18}O. The amount effect is enhanced during moister conditions by the decrease of re-evaporation of those falling raindrops (Pape et al., 2010), and is observed in modern precipitation associated with monsoon systems around the globe, including the Southwest monsoon (Higgins and MacFadden, 2004; Mook, 2006; Lachniet,

2009). On decal to millennial timescales, additional factors are important such as: (1) The ice-volume effect, which is reflects changes in the $\delta^{18}O$ of the ocean due to ice formation and/or glacial melts; (2) Changes in the seasonality of meteoric precipitation, which results in the $\delta^{18}O$ values of the drip-water to be biased toward the $\delta^{18}O$ signal of the season with the highest contribution to the annual amount of meteoric precipitation (Cruz et al., 2005; Johnson et al., 2006; Van Beynen and Febbroriello, 2006); (3) Lastly, shifts in the source of moisture and/or storm tracks which should also be taken into account (i.e., Bar-Matthews et al., 1999, Fleitmann et al., 2003). A poorly ventilated area, located at a significant distance from the cave entrance, provides the ideal environment for recording above-cave environmental changes, as well as, necessary protection from external environmental factors, such as evaporation and temperature variability, which induce kinetic fractionation of the stable isotopes. With such factors obscuring the relationship between MAP $\delta^{18}O$ values and MAT, Dorale et al. (1998) proposed that all strict paleotemperature reconstructions must assume that neither the moisture source nor the seasonality of precipitation has varied significantly through time. Aside from above-cave climate, many secondary processes are potentially involved in producing the stalagmite calcite $\delta^{18}O$ signal. Kinetic fractionation, mixing of water during residence in the vadose zone, dissolution-reprecipitation, and degassing history can contribute to the $\delta^{18}O$ signal, therefore shifting the climate signal it preserves (Dykoski et al., 2005).

1.3.2. $\delta^{13}C$ of Stalagmite Calcite

Speleothem $\delta^{13}C$ values reflect the amount of water-rock interactions above the speleothem, and can be used as proxies for relative moisture abundance in overlying soils and epikarst because soil respiration rates and plant productivity help define the carbon isotopic compositions of speleothem-forming drip-waters (Springer et al., 2008). Lower values of stalagmite calcite $\delta^{13}C$ generally represent humid climatic conditions while higher $\delta^{13}C$ values are commonly indications of drier climatic conditions (McDermott, 2004). Commonly, speleothem $\delta^{13}C$ values are linked to overlying vegetation because cave drip-waters must first

pass through the overlying soil, the organic matter of which is derived from vegetation respiration (Dorale et al., 1998). The majority of the variations in soil organic matter $\delta^{13}C$ values result from differences in the C_3 and C_4 photosynthetic pathways. A C_3 plant uses the Calvin cycle for the initial steps of photosynthesis, that incorporate CO_2 into organic material, forming a three-carbon compound as the first stable intermediate. C_3 plants are mostly trees, cool-season grasses, and forbs with $\delta^{13}C$ values ranging from -32‰ to -22‰, averaging ~-27‰. A C_4 plant prefaces the Calvin cycle with an alternate mode of carbon fixation, integrating CO_2 into a four-carbon compound with the end product actually supplying CO_2 for the Calvin cycle. C_4 plants are typically warm-season grasses found in tropical and temperate grasslands with $\delta^{13}C$ values ranging from -16‰ to -9‰, averaging ~-12‰ (O'Leary, 1988). Even though $\delta^{13}C$ values are also modified as infiltration water dissolves carbonate bedrock in the epikarst zone, the relative influences of C_3 plants (more depleted) and C_4 plants (less depleted) are maintained (Dorale et al., 1998).

Springer et al. (2008) came to the conclusion that the $\delta^{13}C$ signature in stalagmite BCC-002 (Holocene age) from the present study area, pre-2.1 kyrBP, are not affected by the presence of C_4 vegetation. Observed changes in $\delta^{13}C$ values are attributable to changes in soil productivity and respiration, but not attributable to major changes in C_3 and C_4 abundances. The absence of pre-Holocene Climatic Optimum data prevents interpretation of vegetation types (Springer et al., 2009). Values of $\delta^{13}C$ are more depleted when climate is relatively moist, due to increased soil respiration, and enriched when climate is dry, due to decreased soil respiration (McDermott, 2004). Because stalagmite $\delta^{13}C$ signatures depend on the soil $\delta^{13}C$, which depends on the composition of the soil, a correlation can be expected between a pollen abundance proxy on the same time frame and both the soil $\delta^{13}C$ and stalagmite $\delta^{13}C$ signals. A positive correlation can exist between speleothem $\delta^{13}C$ and trace element ratios, particularly Sr/Ca, because decreased moisture results in the precipitation of calcite, leaving the remaining solution enriched in ^{13}C and Sr (Musgrove and Banner, 2004), even though the correlation

strength is most likely weakened by the differences in biotic ($\delta^{13}C$) *versus* abiotic (Sr/Ca) responses to changes in moisture abundance (Springer et al., 2009). Without additional proxies to correlate, particularly trace element concentrations, it is difficult to define the relative influences contributing to the carbon isotopic composition of stalagmite calcite (Williams et al., 2002).

1.3.3. Trace Element Composition

In addition to stable isotope ratios, speleothem trace element composition ratios can also be used to reconstruct paleoenvironmental conditions. They preserve past hydrological information in the epikarst zone above the drip-water site, such as the balance of precipitation and evaporation in the past (Baker et al., 1997; Fairchild et al., 2000; Springer et al., 2009). More specifically, it is understood that speleothem trace element concentrations typically vary as a function of water-residence time in the epikarst zone, as well as, the overall solubility and biogeochemical activity. They assist in interpreting the magnitude and importance of various controls on the water composition due to the additional complexities that arise from the partitioning of species into $CaCO_3$ (Baker, 1997). Williams (2008) illustrated the division of overlying soil from the underlying epikarst zones in karst and cave hydrology.

The major speleothem trace elements can be divided into three groups: (1) those that frequently substitute for Ca or CO_3 in the $CaCO_3$ mineral lattice (i.e., Sr, Ba, Mg, and U for Ca in aragonite and calcite, and SO_4 for carbonate), (2) those that are incorporated interstitially on a molecular scale in $CaCO_3$ (i.e., PO_4, Na, and F in calcite), and (3) those that are present in fluid or solid inclusions within the $CaCO_3$ mineral, which could be hydrologically significant (Fairchild et al., 2007). The most studied trace elements for speleothem interpretation are Ca, Mg, and Sr, others include Ba, Na, K, Al, Fe, and Mn (Fairchild et al., 2001; Garnett et al., 2004; Motyka et al., 2005; Montero et al., 2000; Springer et al., 2008; Fairchild and Treble 2009). Trace element ratios in speleothems are linked to paleo-cave water chemistry by the partitioning of trace elements into calcite during precipitation. A partition coefficient for species X can be defined in

terms of the ratios of X to Ca in water (Ca_w) and in calcite (Ca_c) as follows: $X/Ca_c = K_X (X/Ca_w)$ (Huang et al., 2001). A partition coefficient (K_X) is influenced by temperature, growth rate, growth mechanism and structural characteristics of growth surfaces, which are indicated to be consistent in the cave environment (Fairchild et al., 2000). This is tested by comparison of paleo-cave waters deposited in a stalagmite in terms of Sr/Ca and Mg/Ca ratios. Karst water compositions are controlled by the dissolution of varying proportions of calcite ($CaCO_3$) and dolomite (~$CaMg(CO_3)_2$), which dissolves much more slowly than calcite (Morse and Arvidson, 2002), leading to Mg/Ca ratios of less than one (Figure 1.3). These sympathetic trace element covariations reflect the water-rock reaction time and can arise through enhanced selective leaching effects with prolonged water-rock contact times or from prior calcite precipitation along the epikarstic flow-path, or perhaps both (Fairchild et al., 2000). For the purpose of interpreting speleothem-based geochemical transects as records of paleoclimate change, one must initially assume that epikarst characteristics are invariant (aside from ground water amount and residence time within).

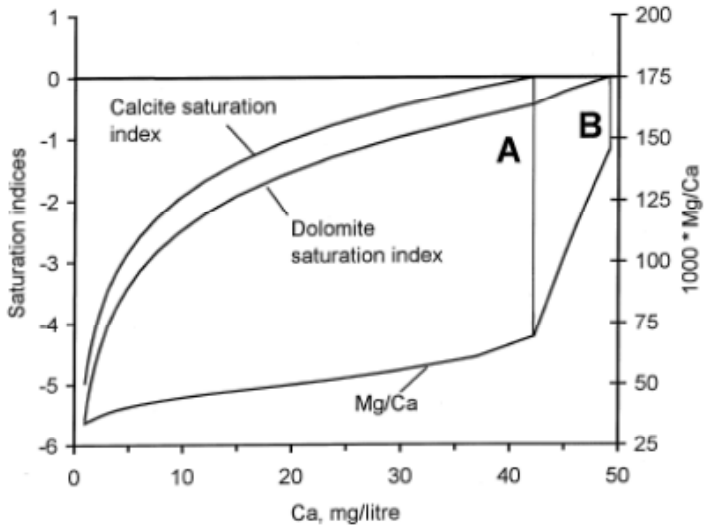

Figure 1.3 Results of a computation to simulate evolution of water chemistry during competitive dolomite and calcite dissolution: (a) position at calcite saturation, (b) position at dolomite saturation (Fairchild et al., 2000).

Shifts to higher Sr/Ca and Mg/Ca ratios are due to increased previous calcite precipitation or selective leaching of Sr and Mg during weathering processes; both of which should be enhanced during dry weather conditions with lower water availability in the karstic environment (Fairchild et al., 2000). When there has been a relative increase in the ratio of dolomite to calcite dissolved during weathering, which is also caused by drier weather leading to longer mean water-rock contact time, higher Mg/Ca concentrations should also be observed. Aside from reflecting the paleohydrology, longer term variations in Sr/Ca and Mg/Ca will also show the past changing source materials (especially soils) and previous karst plumbing. Sr/Ca ratios can be used to reconstruct relative rates of epikarstic moisture transport because low moisture levels can cause longer drip-water residence times, leading to a Ca decrease from calcite precipitation in the overlying epikarst, which then increases Sr/Ca ratios in the underlying speleothems (Springer et al., 2008). Additionally, during periods of low rainfall and low recharge rates, migration of fluids primarily along low-permeability diffuse flow routes increases residence times in the epikarst zone and the interaction between drip-water and carbonate bedrock gives rise to high Sr/Ca ratios (Musgrove and Banner, 2004). In contrast, with higher rainfall and recharge rates, flow path capacities are exceeded and groundwater moves within secondary, high permeability conduits. This lowers the residence time and reactivity, lowering Sr/Ca ratios in stalagmites (Musgrove and Banner, 2004). Likewise, higher $\delta^{13}C$ will result from the preferential loss of ^{12}C during dry periods. During dry (moist) conditions, C_4 (C_3) vegetation thrive, and preferentially take up the heavier ^{13}C (lighter ^{12}C) isotope, resulting in less (more) negative $\delta^{13}C$ values, as well as, decreased (increased) soil respiration. Combining trace element variations with isotope analyses provides a much more powerful approach to resolving single-occurrence paleoclimate events from cyclic paleoclimatological controls. Springer et al. (2008) found that a positive correlation exists between stalagmite Sr/Ca ratios and stalagmite calcite $\delta^{13}C$ values for stalagmite (BCC-002) in Buckeye Creek Cave, southeastern West Virginia.

1.4 Global Paleoclimate

Because the direct measurement of climate variables only spans about one to two centuries back in time, the use of indirect indicators in nature (proxies) to reconstruct past climate is essential. There are only a handful of paleoarchives that preserve both long, continuous records, as well as, records of significantly high resolution. High-resolution, annually resolved paleoarchives, such as tree rings, corals, sediment cores, ice-cores, and speleothems are critical because they preserve a record of conditions at or near timescales of human activity and response, years and decades (Jones et al., 2001; Mann, 2001; Jones and Mann, 2004). These natural paleoarchives record a fragment of climate-related phenomena, either by their biological, chemical or physical nature. Figure 1.4 illustrates the various paleoarchives discussed in this study. To understand the Earth's climate history, these multiple interests must be brought together into a single, seamless story (Bradley, 1999). Reconstructions of past climate based on individual proxies must by calibrated and independently validated against instrumental records within common intervals (Jones and Mann, 2004). All climate

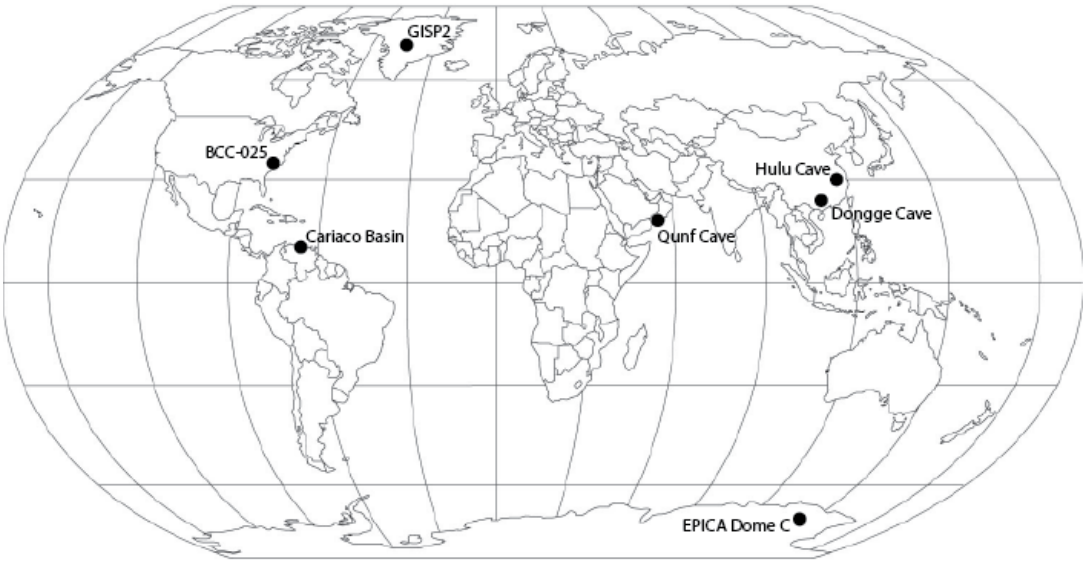

Figure 1.4 Global map illustrating locations of various paleoarchives to be discussed.

reconstructions typically assume implicit long-term stationarity in the nature of a proxy's response to climate (Yuan et al., 2004).

1.4.1. Ice-Cores

Paleorecords developed from ice-cores, most commonly from the polar-ice caps of Antarctica and Greenland, are significant because the multiple isotopic and geochemical signatures preserved within the ice can be used to infer large-scale changes in atmospheric chemistry, circulation, and temperature (Alley, 2000). Predominately, ice-cores serve as a record of atmospheric temperature. Atmospheric gasses, which have homogeneously mixed at the global scale, are often trapped in bubbles within ice, where deuterium and oxygen isotopes can be analyzed (Sowers and Bender, 1995). Additional inclusions, such as wind-blown dust, ash, aerosol concentrations (i.e., De Angelis et al., 1987; Biscaye et al., 1997) and radioactive substances remain trapped in the ice as layers of snow build up, serving as proxies for temperature, precipitation, gas composition of the lower atmosphere, solar variability, ocean volume, sea-surface productivity, volcanic eruptions (i.e., Udisti et al., 2004), desert extent, and forest fires (Yuan et al 2004; Legrand and Mayewski, 1997). After analysis of a high-resolution record of aeolian dust from the EPICA Dome C ice-core, Lambert et al. (2008) noticed a significant correlation between dust flux and temperature records during glacial periods, that was absent during interglacial periods (Figure 1.5). Some ice-cores preserve annual layers that can be counted in order to determine an absolute age chronology (Alley et al., 1997; Thompson et al., 1998). However, ice flow may compact and disrupt layers previously deposited, requiring additional lines of evidence to discern its chronology (Alley et al., 1995). Ice-core time resolution depends on the amount of annual snowfall, and reduces with depth, as compaction renders deeper layers thin and annual layers indistinguishable.

Few records span as far back as the Pleistocene, one in particular is the European Project for Ice Coring in Antarctica (EPICA) from Dome C, Antarctica (coordinates 75°06'S; 123°21'E, 3233m above sea level). EPICA Dome C is the longest undisturbed ice-core record,

where ice has been sampled to an age of ~800 kyrBP, revealing 8 previous glacial cycles (Figure 1.5). Deuterium and oxygen isotopes from EPICA Dome C indicate that interglacial stages between 800-450 kyrBP (MIS 19-13) had less pronounced warmth than the interglacial episodes that have occurred during the past 450 kyr (MIS 11-1) (Jouzel et al., 2007). Brook (2005), and Siegenthaler et al. (2005) also characterize various systematic long-term as well as millennial changes revealed in the EPICA Dome C ice-core. The magnitude of interglacial peaks in the EPICA sequence is matched by greenhouse gas concentrations, with cooler interglacials coinciding with lower levels of CH_4 and CO_2. These levels can also be identified in sea surface temperatures (Becquey and Gersonde, 2002), and long speleothem records (Winograd et al., 1997). Other climate proxies suggest that interglacials during the Middle Pleistocene (~780-450 kyr) were as warm as interglacials into the Late Pleistocene (<450 kyrBP). This pattern of interglacial warmth is consistent in sea-surface temperature records from the North Atlantic

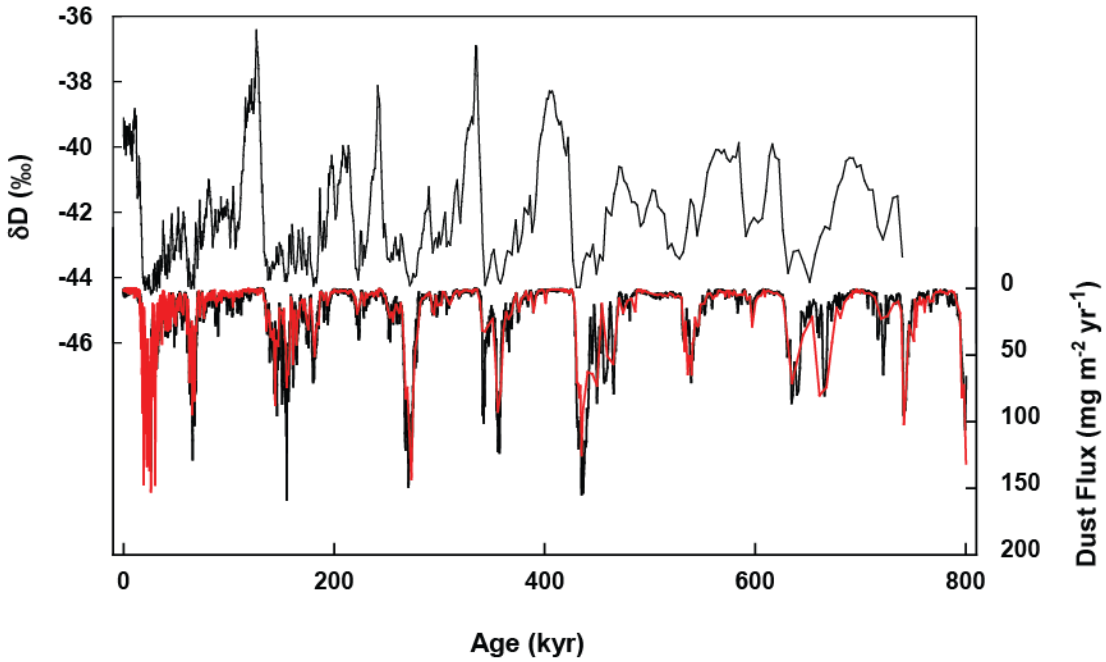

Figure 1.5 EPICA Dome C ice-core, Antarctica. Stable isotope (δD) (Jouzel et al., 2007) and dust flux records (mg m^{-2} yr^{-1}). Red line represents Coulter Counter (55 cm to 6 m resolution); Black line represents Laser-Scattering data (55 cm mean) (Lambert et al., 2008).

region, but is in strong contrast with records from Antarctica and the Southern Ocean where temperatures of early Middle Pleistocene interglacials are consistently cooler than those of interglacials in the last 450 kyr (Candy et al., 2010).

The Greenland Ice Sheet Project (GISP-2) ice-core record represents the most accepted reconstruction of atmospheric temperature for high-latitude paleoclimates spanning the last ~110 kyr. GISP-2 shows highly variable late Pleistocene temperature fluctuations followed by relatively stable Holocene conditions (Grootes et al., 1993; Alley, 2000). Changes in the formation of the North Atlantic Deep Water (NADW) are thought to account for some of the more defined climatic events in the ice-core records, with some shifts as large as 8°C (Severynghaus et al., 1998). GISP-2 also exemplifies two dramatic climate changes, the Younger Dryas and the 8200-year event (Chapellaz et al., 1993) (Figure 1.6). The Younger Dryas, the "Big Freeze", was a geologically brief (~1.3 kyr) period of cold climatic conditions and drought between ~12.8-11.5 kyrBP, widely thought to have been initiated by the collapse of the North American ice-sheets (Berger, 1990; Muscheler, 2008). The 8200-year event represents a sudden decrease in global temperatures, much milder than the Younger Dryas that occurred

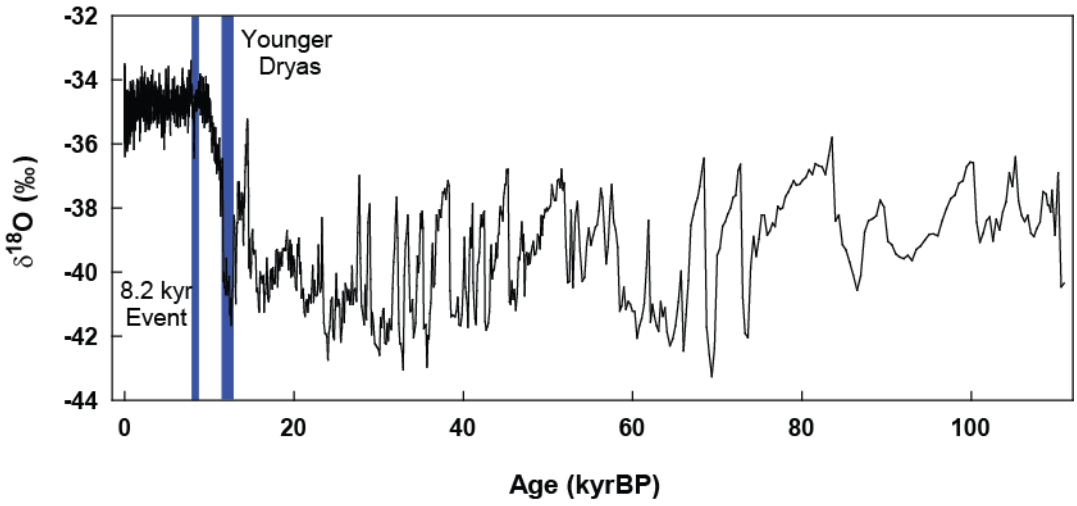

Figure 1.6 GISP-2 ice-core, Greenland. Stable isotope ($\delta^{18}O$), two meter record (Grootes et al., 1993; Steig et al., 1994; Meese et al., 1994; Stuiver et al., 1995). Climatic events, 8,200-year and Younger Dryas, shown with blue bars.

~8.2 kyrBP, lasting ~2-4 centuries. The cooling was a significant exception to the general trends of the Holocene climate, where atmospheric methane decreased drastically (Kobashi et al., 2007).

1.4.2. Asia Speleothem Records

Speleothem time series contain evidence of the changing climate system and sometimes of specific forcing factors. The records are inherently more complex than ice-cores. The speleothem records from the monsoon-sensitive regions have yielded the most highly-resolved paleoclimate reconstructions, which also correlate with the GISP-2 record (Cheng et al., 2009a). $\delta^{18}O$ records of speleothem calcite obtained from caves in China (Wang et al., 2005) and Oman (Fleitmann et al., 2003) suggest that strong climatological changes have occurred in Asian monsoon intensity over the last several millennia (Cheng et al., 2009b). The correlation of speleothem records from cave sites associated with the Asian monsoons to a marine record of ice advance and retreat in the North Atlantic (Bond et al., 2001; Cosford et al., 2008) provides a suggestion of widespread century-scale climate changes resulting in different local manifestations.

Stalagmite calcite $\delta^{18}O$ records from Hulu Cave and Dongge Cave, China, demonstrate that Asian monsoon intensity typically follows changes in solar insolation, shifts in sea level and internal climatic circulation, a response similar for a large area of China (Wang et al., 2001; Dykoski et al., 2005) (Figure 1.7). Asian monsoons are important heat and moisture transporters from the Western Pacific Warm Pool to the northern hemisphere. The Hulu/Dongge records indicate major and abrupt changes in the proportion of tropical and subtropical precipitation reaching China, which correlate with temperature in the North Atlantic region as recorded in Greenland ice, implying that Asian monsoon intensity is dictated by the same processes affecting Greenland air temperatures (Yuan et al., 2004). Changes in the North Atlantic Deep Water have been proposed to explain shifts in the Greenland air temperature

(Broeker, 1994). Atmospheric circulation, oceanic circulation, and solar insolation may be responsible for the Hulu Cave record (Porter and An, 1995).

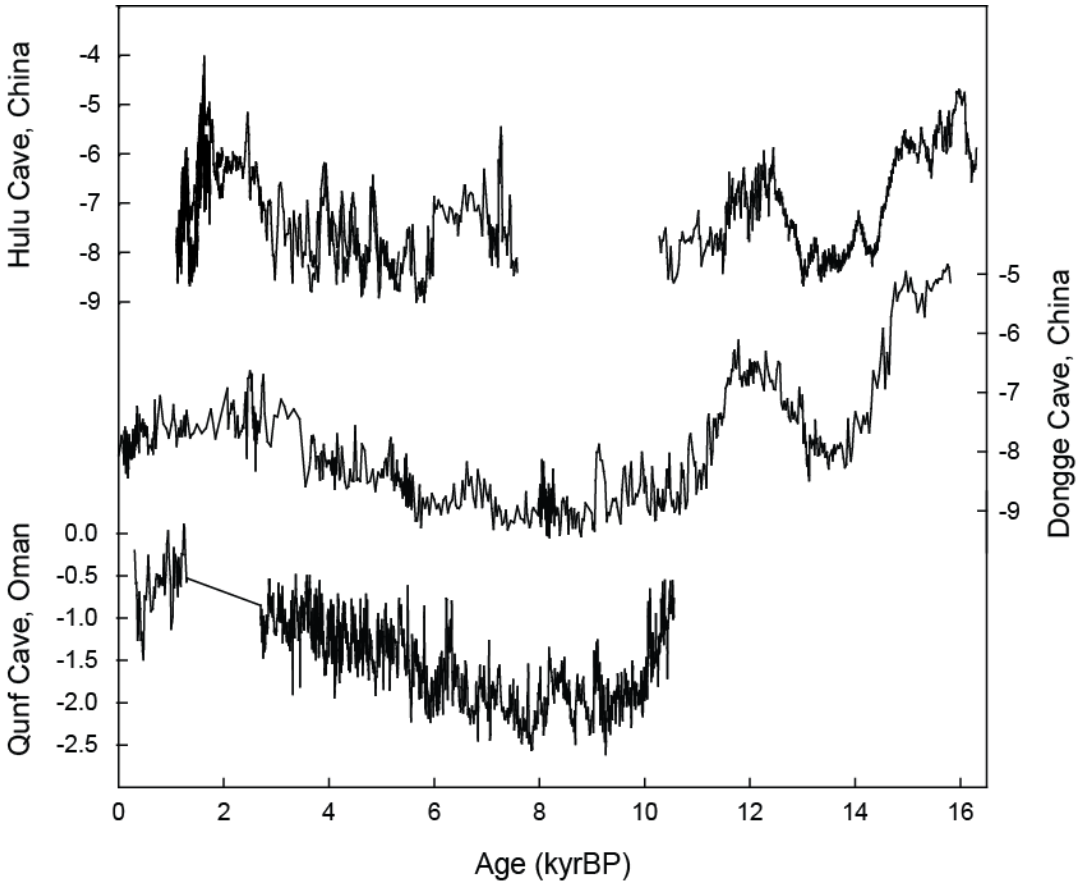

Figure 1.7 Speleothem $\delta^{18}O$ records from Hulu Cave, China, Dongge Cave, China, and Qunf Cave, Oman.

Indian Ocean monsoon records reveal that increasing air temperatures in the northern Atlantic region correlate with an increase in Indian Ocean monsoon precipitation; decreases in precipitation correlates with cooling events recorded in the GISP-2 ice-core. Isotopic signatures analyzed in stalagmite calcite from southern Oman, reveal that the transport of heat and moisture to higher latitudes by the IOM is variable and largely dictated by glacial boundaries (Neff et al., 2001; Fleitmann et al., 2003). The comparative study by Fleitmann et al. (2003) suggests that modern precipitation in the northern tropics is affected by the weakening of

monsoons on a widespread (global) scale, with summer solar insolation acting as the driving force.

1.4.3. Marine Sediments

During the last glacial period, the climate of the Northern Hemisphere was characterized by rapid, large-amplitude temperature fluctuations of ~2-3 kyr cycles. These fluctuations are apparent in Greenland temperature reconstructions and corresponding temperature and hydrological variations have been documented by marine sediments in the Northern Hemisphere (Asmerom et al., 2010). Marine sediments preserve records of paleoclimate and paleoocean organic variability (i.e., sea-surface temperature, salinity, chemistry, sediment transport), but due to low sedimentation rates and the effects of bioturbation, most marine records do not preserve subcentennial-scale paleoceanographic variability.

For understanding low-latitude paleoclimate changes over the last glacial/interglacial cycle, the Cariaco Basin marine sediment record possesses an extensive, relatively high level of temporal resolution, largely because of its unique environment of deposition, an isolated basin on the continental shelf of northern Venezuela (Dean and Piper, 1999; Hughen et al., 2004) (Figure 1.8). Cariaco Basin sedimentation shows seasonal patterns of deposition of the last 14.5 kyr, preserved by anoxic bottom waters (Hughen et al., 1996; Haug et al., 2001). The geochemical record consists of down-core concentrations of Fe and Ti which are thought to reflect changes in terrigenous sediment input and thus, river volume and precipitation amounts with lack of diagenetic control (Peterson et al., 2000). Haug et al. (2001) interpreted down-core changes in bulk geochemistry of the Cariaco Basin sediments to reflect changes in the latitudinal position if the Inter-Tropical Convergence Zone (ITCZ), which represents the zone of confluence of the southern and northern trade winds, and is marked by low pressure and high precipitation. Peterson and Haug (2006) provide evidence to suggest that when North Atlantic sea-surface temperatures are below-average, detrital input from nearby rivers is also below-

average, indicating that the ITCZ is anomalously to the south of its average position. During boreal winter, when the ITCZ is at its southernmost position, intense upwelling, and higher productivity can be observed in the Cariaco Basin (Ziegler et al., 2008). Similarly, when the

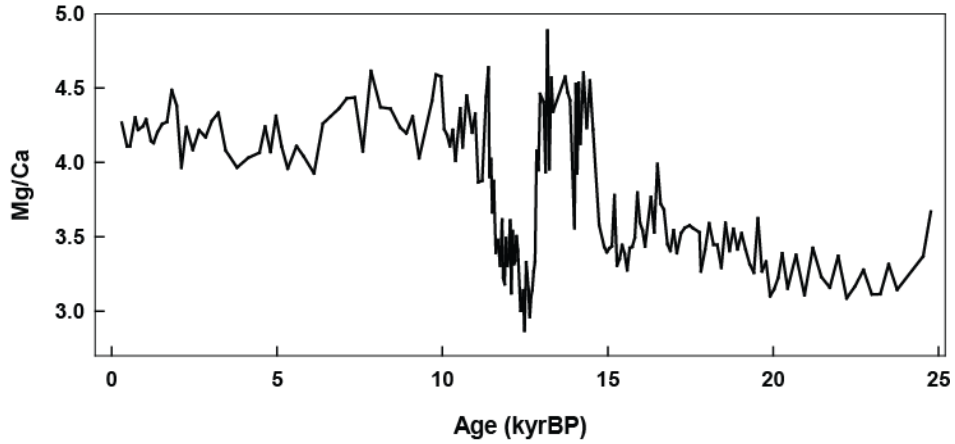

Figure 1.8 Cariaco Basin forminiferal Mg/Ca ratios (Lea et al., 2003).

North Atlantic sea-surface temperature is above-average, an increase in detrital material is observed during summer, indicative of a more northerly location of the ITCZ. The input of terrestrial detritus provides a definitive history of ITCZ movements, more so than the reconstruction of past upwelling and biological input. A correlation of the Cariaco Basin to the ITCZ position may be evidenced by the movement of Caribbean waters into the Gulf of Mexico (GOM). As the ITCZ moves north of the equator during the North American Summer, so does the transport of moisture into northern Mexico and southwestern United States (i.e., North American Summer Monsoon).

LoDico et al (2006) illustrates decadal-to-centennial-scale climatic change from ~10.5-7 kyrBP in the GOM with an overall warming of about 1.5°C and six major climatic oscillations. This is documented with Mg/Ca, $\delta^{18}O_{calcite}$ (a proxy for temperature) and inferred $\delta^{18}O_{saltwater}$ (a function of ice volume and salinity) by utilizing foraminiferal calcite. The 8,200-year event discussed earlier is evidenced in this record by a change in salinity and biotic communities preceded by major freshwater input from ~8.6-8.3 kyrBP. Another freshwater input is evidenced

by planktonic foraminifera as melt water from the Laurentide ice-sheet ~14-10.2 kyrBP (Poore et al., 2003). The GOM reached optimum temperatures ~9-7 kyrBP although low latitudes show this warming earlier; an event explained by a lingering influence of the Laurentide Ice Sheet on North America during the early Holocene (Mitchell et al., 1988).

1.4.4. Global Insolation

The perturbations in the Earth's orbital parameters change sufficiently the latitudinal distribution and seasonal pattern of insolation (a measure of the amount of solar radiation energy) received at the top of the atmosphere (Berger and Loutre 1994). The shape of the Earth's orbit changes from a nearly perfect circle to an oval shape on ~100 kyr cycle (eccentricity). The Earth's axis is tilted at an angle that varies 22°-24° every ~41 kyr (obliquity). Lastly, the Earth wobbles on its axis as it spins, with a periodicity of ~19-23 kyr (precession) (Figure 1.9). These small variations in Earth-Sun geometry change how much sunlight each hemisphere receives and how extreme the seasonal changes are. Changes in glacial variability are not characterized by any single or sudden transition; rather, they exhibit a steady progression. The mean, variance, skewness, and timescale associated with the glacial cycles all show an approximately linear trend over the last 200 kyr (Huybers, 2007). The Milankovitch theory is a particular version of this broad astronomical theory of paleoclimates, where Milankovitch used caloric seasons to explain the long-term climatic variations during the Quaternary (Berger, 1988). Evidence supporting the Milankovitch theory first emerged from a series of fossil coral reefs that formed on a shallow ocean bench in the South Pacific during warm interglacial periods (Pandolfi, 1996). Because of the decaying uranium in the coral, the time resolution of these reefs is well-defined (Stein et al., 1993). They recorded the millennia between ice ages, and the maximum length of each ice age, corresponding with where Milankovitch predicted.

The Pleistocene was marked by major ‘‘glacial/interglacial’’ oscillations in global ice volume, at timescales of tens to hundreds of millennia. These oscillations appear similar to timescale changes in the distribution of insolation over the Earth’s surface related to long-term changes in the orbital position of the Earth relative to the Sun (Jones and Mann, 2004). Huybers (2007) found that cycle skipping is frequent during the late Pleistocene, where most deglacial events are separated by two or three obliquity cycles, corresponding to 80 kyr or 120 kyr glacial cycles which average to the 100 kyr eccentricity variability.

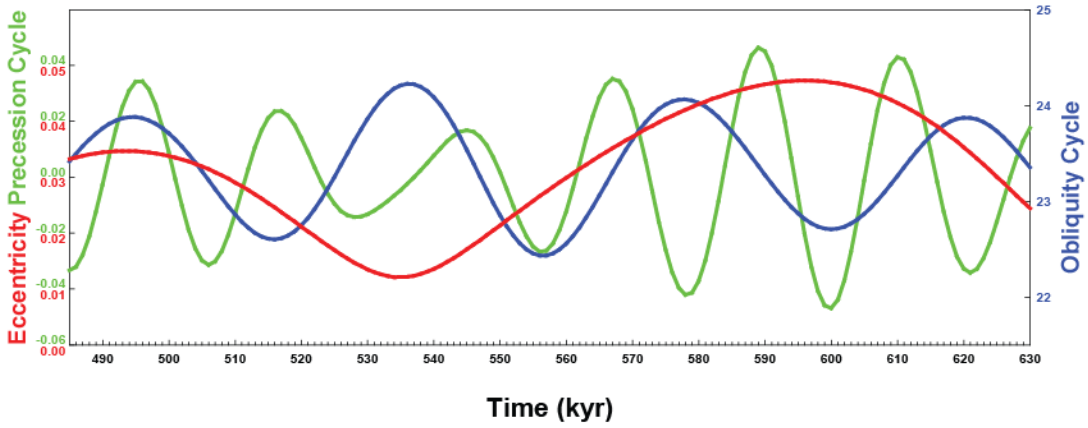

Figure 1.9 Eccentricity (~100 kyr), obliquity (~41 kyr), and precession (~19-23 kyr) cycles during time of BCC-025 growth (~490-630 kyrBP).

1.5 Geologic Setting

A calcite stalagmite (BCC-025) was recovered from Buckeye Creek Cave (BCC), located in Greenbrier County, southeastern West Virginia (Figure 1.10). The cave is developed within the massive limestone of the Mississippian-age Greenbrier Group, with an overlying escarpment comprised of Mississippian-age sandstones, siltstones, and shales (Springer, 2002). Locally, thickness of these formations varies from 350 m to 122 m with a regional strike of N 30° E and an average dip of 3° NW (Dasher and Balfour, 1994). The Greenbrier Limestone, named for its exposure along the Greenbrier River, extends from the southern portions of Pennsylvania to Maryland, Virginia, and West Virginia. This massive, dark gray-blue

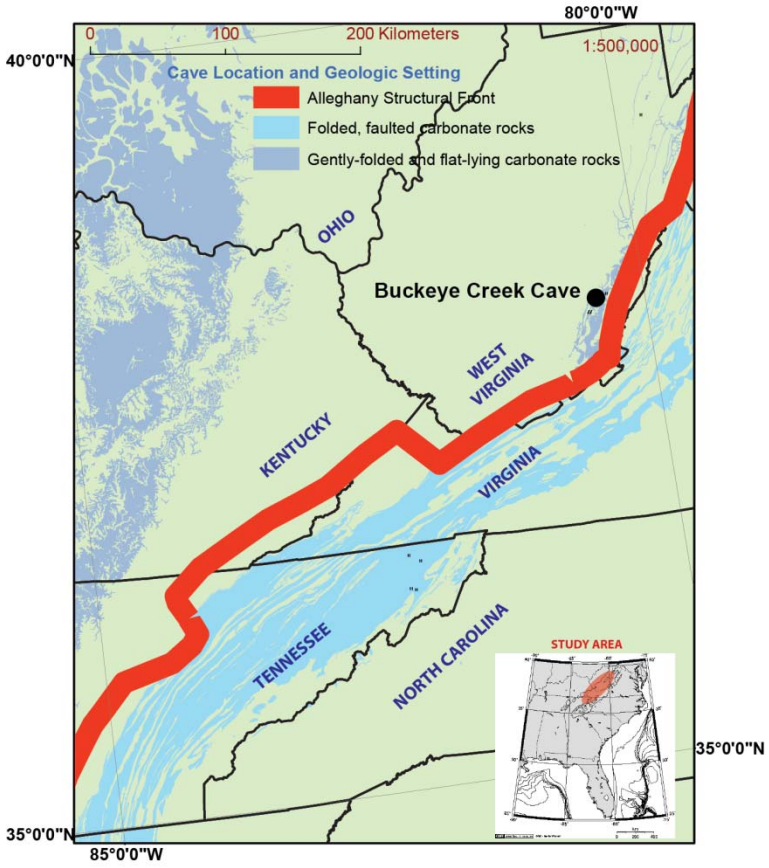

Figure 1.10 Location map of Buckeye Creek Cave, Appalachian Mountains, southeastern West Virginia.

limestone is characterized by various land depressions, such as sinkholes, an abundance of caves, underground streams, and many oxbow river channels (Springer et al., 2003). Karst develops from the dissolution of limestone by large quantities of moving groundwater to dissolve the rock and form underground passages. The volume of groundwater depends directly on the porosity and permeability of the aquifer. Presently, BCC is the sole outlet for the topographically enclosed Buckeye Creek basin, with a catchment area of 14 km^2 (Springer and Wohl, 2002). BCC is within the Greenbrier River watershed, a major tributary of the westward-flowing New River and across the Eastern Continental Divide from the eastward-flowing Potoman and James Rivers. The Greenbrier River watershed is moderately hilly with a maximum relief of 85 m in the

eastern part of the basin and 215 m in the west. Butler Mountain borders the basin in the northwest, while Spring Creek borders the basin to the northeast and east. Springer et al. (2009) found that the Greenbrier River aggraded no later than the Early Holocene and may have begun aggrading during the Late Pleistocene. Wynn and Read (2006) compiled a regionally-scaled, detailed stratigraphic column from well cuttings, which illustrates the extent of shallow-water carbonates and siliclastic units in the Greenbrier Limestone.

The mountainous, humid, temperate region of eastern North America that is chosen as the study area is well-suited because of 1) the demonstrated response of regional climate to variability in the North Atlantic Oscillation (NAO), Atlantic Multidecadal Oscillation (AMO), El Niño-Southern Oscillation (ENSO), and Pacific Decadal Oscillation (PDO) (Enfield et al., 2001; McCabe et al., 2004; Seager, 2007), 2) the quality and quantity of caves that possess actively-growing speleothems, 3) the exceptional access to caves, 4) the potential to obtain inactive speleothems that are pre-Holocene in age, and 5) the ability to establish drip-water and environmental monitoring stations at multiple sites within several cave systems (Springer et al., 2008).

CHAPTER 2

METHODS

2.1 Sampling

BCC-025 was collected from Buckeye Creek Cave, Appalachian Mountains, southern West Virginia. The speleothem was located in an isolated chamber on the second level of Buckeye Creek Cave, approximately 25 m below the surface and >1 km from the entrance, minimizing surface effects on cave temperature and humidity (White, 2004). The stalagmite is a total of 49 cm in length, tan in color, consisting of fibrous calcite, with a chalky rind, and is quite dense (Figure 2.1). The speleothem was cut perpendicular to the axis of growth with a continuous-rimmed diamond blade and polished with a hand-held, water-spray polisher. A transparent ruler was taped along the growth axis to simplify drilling measurements. The speleothem was then drilled contiguously to the growth axis at 0.5 mm increments using a hand held milling tool (DREMEL, 400-XPR) equipped with a titanium bit (H1.11.005 #1/4). Sample powders, a total of 980, were stored in labeled micro-centrifuge tubes. Using sample increments of 0.5 mm yields a time interval that ranges from a few years to a few hundred years for each sample, depending on the growth-rate (McDermott, 2004).

2.2 Geochronology

Radiometric age constraints were provided by $^{234}U/^{230}Th$ dating techniques developed for carbonates (Broecker, 1963) and adapted for measurement on an inductively coupled plasma mass spectrometer (Edwards et al., 1987; Shen et al., 2002) at the University of Minnesota. Calcite powder was sampled using a dental drill with a 0.9mm diameter tungsten-carbide drill bit. Top and bottom $^{234}U/^{230}Th$ dates were obtained along the growth axis of stalagmite BCC-025, revealing that calcite growth began ~628,321 (± 80.541 kyr) years ago

and stopped ~488,777 (± 20.693 kyr) years ago. The dates reveal that stalagmite BCC-025 formation began beyond the accepted range of the dating technique (before 600 kyr) (Lundberg et al., 2010). An age model was constructed by linear interpolation between the two $^{234}U/^{230}Th$ ages to create a radiometric timescale for isotope and trace metal measurements.

2.3 Stable Isotope Analysis

Using a Sartorius microbalance, each sample powder was weighed at a range of 200-225 µg and placed into individual LABCO Exetainer vials. Each sealed Exetainer vial was helium-purged, manually acidified with 100‰ phosphoric acid to dissolve carbonates, and equilibrated at 50°C for 12 hours. Samples were analyzed using a GasBench II with GC-PAL auto-sampler, and ThermoFinnigan DeltaV isotope-ratio mass spectrometer (IRMS). One in every 50 samples was analyzed in triplicate, to demonstrate reproducibility. Isotopic values, $\delta^{13}C$ and $\delta^{18}O$, were standardized to V-PDB using an in-house reference (UTAH) that is standardized V-PDB. The average standard deviations in BCC-025 triplicates were 0.217‰ and 0.143‰ for $\delta^{13}C$ and $\delta^{18}O$, respectively. Isotopic values are expressed in per mil (‰) with the following equations:

$$\delta^{13}C = [(({}^{13}C/{}^{12}C)_{SAMPLE} - ({}^{13}C/{}^{12}C)_{STANDARD}) / ({}^{13}C/{}^{12}C)_{STANDARD}] \times 1000$$

$$\delta^{18}O = [(({}^{18}O/{}^{16}O)_{SAMPLE} - ({}^{18}O/{}^{16}O)_{STANDARD}) / ({}^{18}O/{}^{16}O)_{STANDARD}] \times 1000$$

2.4 Trace Element Analysis

The Brüker ARTAX µ-XRF was used to scan BCC-025 for Sr/Ca trace elemental abundances along the growth transect, to the immediate right of the drilled isotope transect. Instrument settings were as follows: Beam size: 70 mm; X-ray tube: Pt; Voltage: 50 kV; Current: 600 mA; Filter: Al-Ti-Cu; Conditions: Air; Ca and Sr Lines: Ka.

The full range of uninterrupted transect scanning distance is ~4.0 cm, requiring that multiple transect ratios be pieced together. While a calibration for converting the Sr/Ca count ratios to elemental ratios has been developed (Buckles et al., 2011), the raw count ratios are used here for simplicity.

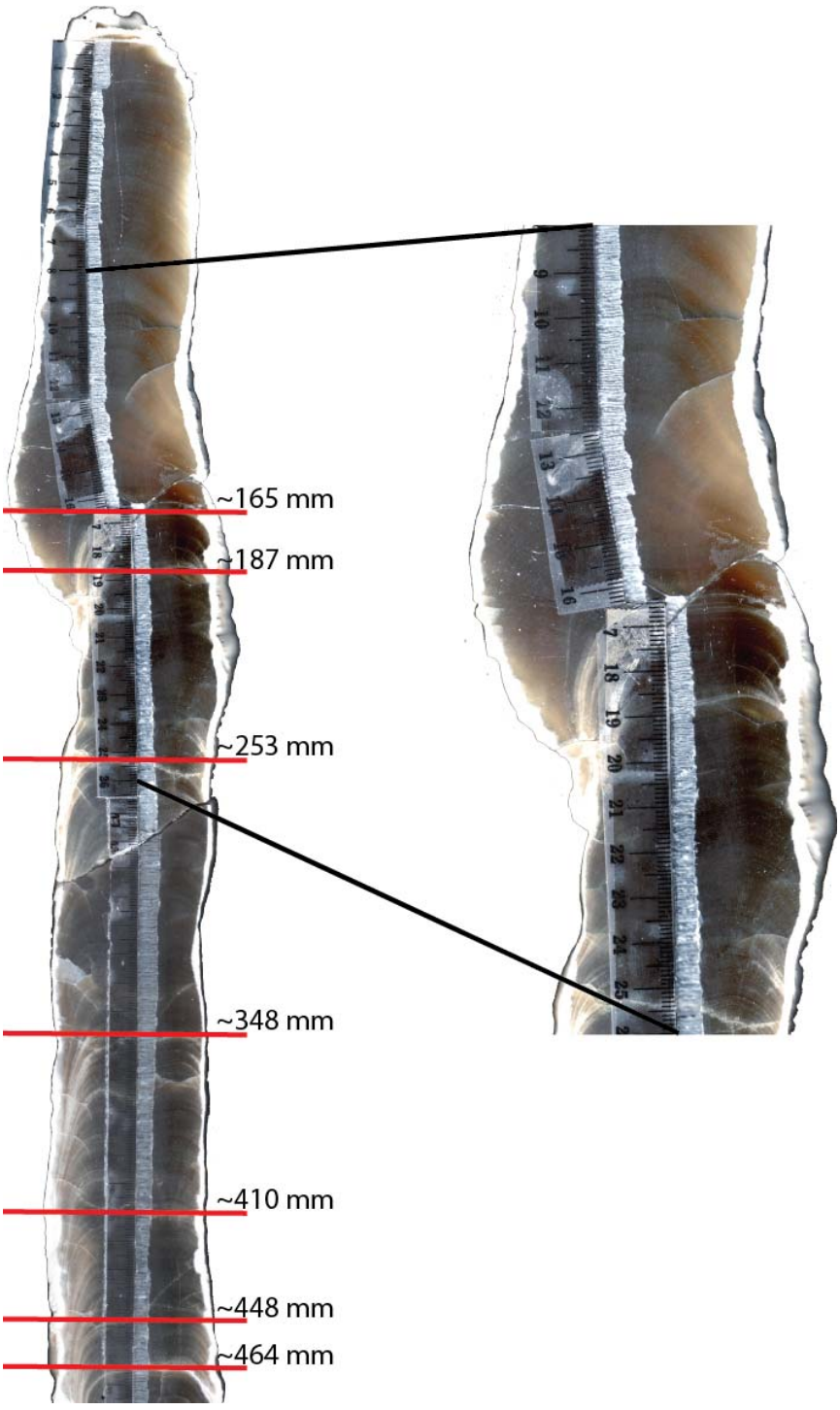

Figure 2.1 Scanned image of stalagmite BCC-025. Total length: 490 mm, milled at 0.5 mm increments. Approximate visual location of growth hiatuses in red. Enlarged section to show detail.

CHAPTER 3

RESULTS

3.1 $\delta^{18}O$ Record in Stalagmite BCC-025

Throughout the entire record (~630-490 kyrBP) spanning 490 mm, BCC-025 $\delta^{18}O$ ranges from approximately -7.6‰ to -4.9‰, an overall range of ~2.7‰ (Figure 3.1 A-W). From the bottom of the record (490 mm), upward through 334mm, $\delta^{18}O$ ranges from approximately -6.8‰ to approximately -4.9‰, an overall range of ~1.9‰. During this interval, the $\delta^{18}O$ record exhibits a decreasing trend, punctuated by one major episode of enrichment/depletion (Figure 3.1). Within this major episode are seven smaller enrichment/depletion events (A-G). Two short 0.6‰ depletion events occurred from ~490-468 mm (Figure 3.1 A-B), followed by a 2.0‰ enrichment event. Between ~450 mm and ~410 mm, 2.5‰ depletion occurs just before the first major enrichment/depletion episode (Figure 3.1 C-F). For ~30 mm, from ~410-380 mm, $\delta^{18}O$ is enriched 1.1‰. A 0.8‰ depletion between ~380 mm and ~360 mm ends the first major episode (Figure 3.1 G), gradually leading into a 0.6‰ enrichment between ~360 mm and ~344 mm.

From ~334 mm to the end of the $\delta^{18}O$ record (0mm) in BCC-025, values range from approximately -7.6‰ to approximately -5.6‰, an overall range of ~2.0‰ (Figure 3.1 H-W). During this interval, the $\delta^{18}O$ record exhibits overall enrichment, punctuated by four major episodes of enrichment/depletion. Within these four major episodes lie sixteen smaller enrichment/depletion events. The first major episode is initiated with a zone of -7.6‰ depletion (Figure 3.1,H); then, from ~324 mm through ~270 mm, a gradual 1.0‰ enrichment of $\delta^{18}O$ (Figure 3.1 I-K), followed by a sudden 2‰ enrichment. Between ~250 mm and ~240 mm, a

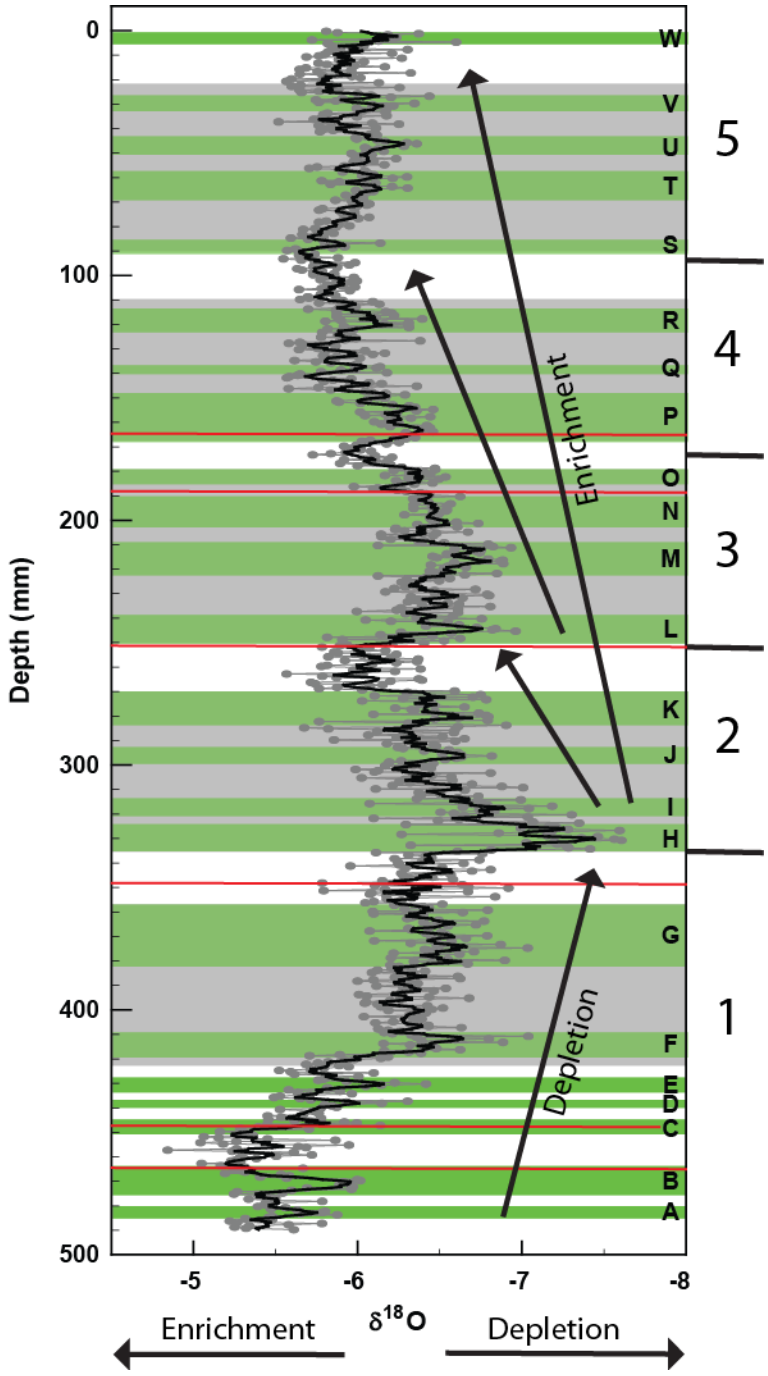

Figure 3.1 Enrichment/depletion episodes recorded in BCC-025 reflected by $\delta^{18}O$. 5-point average (bold black line), growth hiatuses (red lines), major enrichment/depletion episodes (gray bars, numbered on right) and minor enrichment/depletion episodes (green bars, corresponding letters A-W).

1.4‰ depletion (Figure 3.1 L) leads into the second major episode, with a 0.7‰ enrichment. After a 0.9‰ depletion (Figure 3.1 M), three gradual ~1.0‰ enrichments between ~210 mm and ~90 mm occur before the last major episode (Figure 3.1 N-R). The fourth major episode of enrichment/depletion is characterized mostly by a gradual 0.76‰ depletion from ~90 mm to 45 mm (Figure 3.1 S-U), and immediately after, a less gradual 0.4‰ depletion between ~45 mm and ~25 mm (Figure 3.1 V). From ~25 mm to ~5 mm, a 0.5‰ enrichment occurs, followed by a 0.5‰ depletion (Figure 3.1 W) where growth of stalagmite BCC-025 ceased.

3.2 $\delta^{13}C$ Record in Stalagmite BCC-025

Throughout the entire record, $\delta^{13}C$ ranges from approximately 0.0‰ to approximately -5.5‰, an overall range of ~5.5‰. Six major episodes of enrichment/depletion are observed in this $\delta^{13}C$ record (Figure 3.2). From 490 mm to ~470mm, there is a 1.8‰ depletion in $\delta^{13}C$, followed by an abrupt 3.8‰ enrichment at ~476 mm, just before a comparable 4.4‰ depletion from ~476-450 mm (Figure 3.2 A-C). From ~450-415 mm, four enrichment episodes (2.1‰, 1.0‰, 1.5‰, 1.0‰, respectively) lead into the second major episode (Figure D-F). Between ~360mm and ~260mm, the second major episode is largely a ~1.7‰ depletion episode that can be further divided into seven minor enrichment/depletion events (Figure 3.2 G-L). The next ~20 mm are characterized by a ~1.5‰ enrichment that, in the subsequent ~10 mm, gradually dissipates into ~1.0‰ depletion (Figure 3.2 M-O). $\delta^{13}C$ values steadily climb to a ~2.1‰ enrichment over ~60 mm, from ~230-170 mm. Throughout the next ~40 mm, two large $\delta^{13}C$ depletions occur (~2.8‰ and ~3.0‰, respectively), followed by an abrupt 2.3‰ enrichment from ~190-170 mm (Figure 3.2 P-Q). The fifth major episode, characterized by four individual enrichment/depletion events, is predominantly a ~1.7‰ depletion of the $\delta^{13}C$ record (Figure 3.2 R-R3). A ~2.0‰ depletion, surrounded by two ~1.5‰ enrichments, separates the last two major episodes (Figure 3.2 S). The uppermost-defined episode of $\delta^{13}C$ can be subdivided into seven

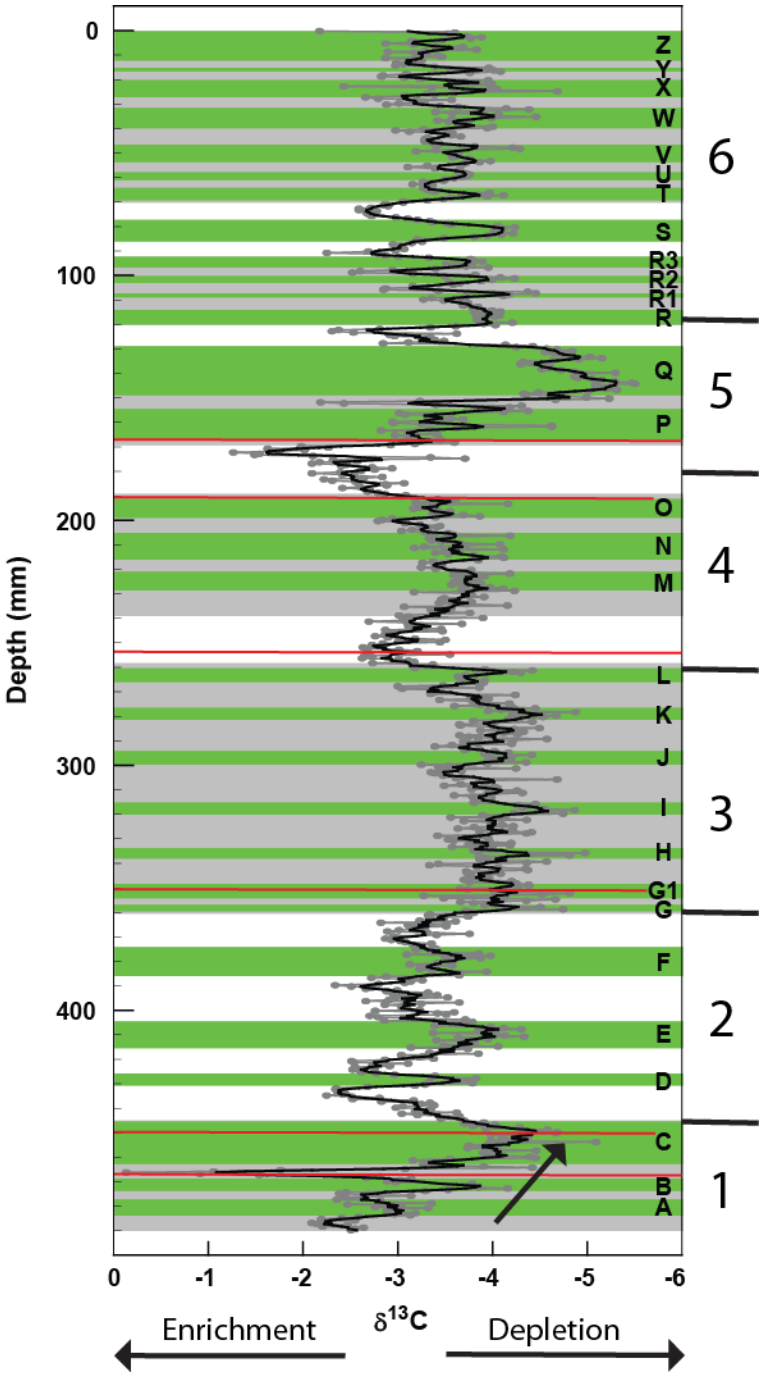

Figure 3.2 Enrichment/depletion episodes recorded in BCC-025 reflected by $\delta^{13}C$. 5-point average (bold black line), growth hiatuses (red lines), major enrichment/depletion episodes (gray bars, numbered on right) and minor enrichment/depletion episodes (green bars, corresponding letters A-Z).

smaller events, with very small amplitudes. Overall, this major episode is a ~1.4‰ depletion from ~70 mm until the cessation of BCC-025; providing a $\delta^{13}C$ signal considerably more stable than the previous ~420 mm (Figure 3.2 T-Z).

3.3 Trace Element Record in Stalagmite BCC-025

Throughout the entire record (~630-490 kyrBP) spanning 490 mm, Sr/Ca ratios range from ~7.5 to ~2.0, an overall range of ~5.5. The trace element record can be divided into two primary enrichment/depletion episodes, subdivided into six smaller episodes (Figure 3.3). The first primary episode includes four major episodes; from the beginning of the record (490mm) through ~167 mm, Sr/Ca ratio ranges from approximately ~7.5 to approximately ~2.0, an overall range of ~5.5 (Figure 3.3 A-L). This interval illustrates a large and abrupt increase in Sr/Ca at ~480 mm, again at ~365 mm, leading into the second interval at ~167 mm. Beginning in the first major episode (~490-480 mm) Sr/Ca increases ~2.0, abruptly decreases ~2, and increases ~2.0 again (Figure 3.3 A-B). The second major episode illustrates four enrichment/depletion events over ~100 mm, with an overall, gradual increase (~2.5) (Figure 3.3 C-F). Within the next ~15 mm, Sr/Ca decreases ~1.5. Within the third major episode, Sr/Ca increases ~2.7 over ~30 mm (Figure 3.3 G), decrease ~1.0, then show subsequent ~1.0 increases (Figure 3.3 H-I). The fourth major episode, with three minor enrichment/depletion events, decreases ~6.0 from ~260-167 mm (Figure 3.3 J-L).

The second primary episode includes three major episodes; from ~167 mm to the top of the stalagmite BCC-025 (0 mm), Sr/Ca ratio counts range from approximately ~6.8 to approximately ~2.0, an overall range of ~4.8 (Figure 3.3 M-V). The first major episode in this interval (~167-150 mm) shows two abrupt increases, ~5.0 and ~3.0, respectively (Figure 3.3 M-N). After an immediate ~2.2 decrease (~150-135 mm), the second major episode (~135-70 mm) is a period of stable ~2.1 increase (Figure 3.3 O-R), which rapidly decreases ~2.3 over the next 15 mm. There is a slight ~0.8 increase, followed by ~0.6 decrease before the third major

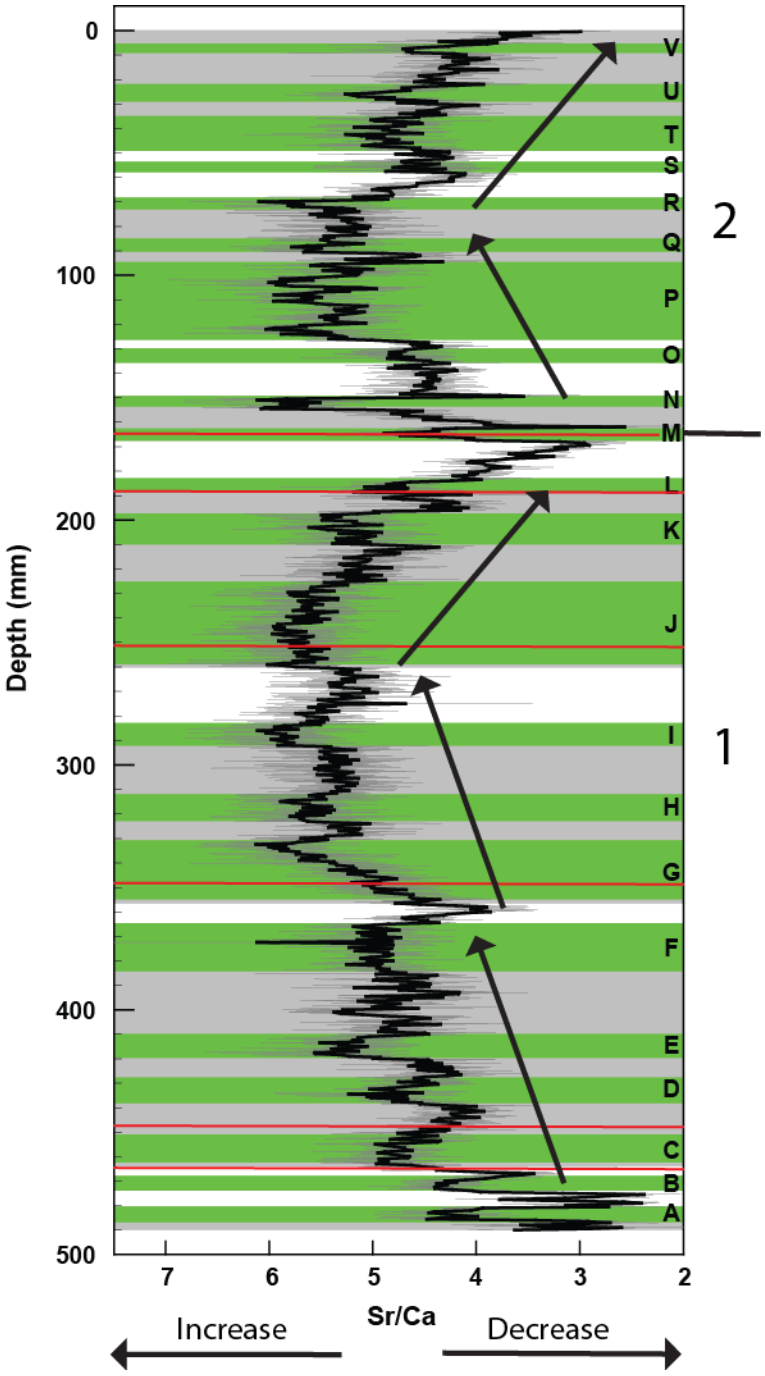

Figure 3.3 Enrichment/depletion episodes recorded in BCC-025 reflected by Sr/Ca ratio. 5-point average (bold black line), growth hiatuses (red lines), major enrichment/depletion episodes (gray bars, numbered on right) and minor enrichment/depletion episodes (green bars, corresponding letters A-V).

episode (Figure 3.3 S), initiated by a ~2.3 increase (Figure 3.3 T). The final major episode contains three smaller enrichment/depletion events, illustrating an overall ~2.6 decrease just before the cessation of BCC-025 at 0 mm (Figure 3.3 T-V).

3.4 Stalagmite BCC-025 Isotope Geochemical Correlations

Values of $\delta^{18}O$, $\delta^{13}C$, and Sr/Ca from BCC-025 are not characterized by a high degree of covariance throughout most of the record (Figure 3.4). Between 490 mm and ~463 mm, all records preserve two episodes of enrichment/depletion (Figure 3.4 A). Both stalagmite $\delta^{18}O$ and $\delta^{13}C$ records show corresponding depletion/enrichment events between ~440 mm and ~428 mm (Figure 3.4 B), a corresponding zone of depletion at ~ 420-410 mm (Figure 3.4 C), and a corresponding zone of multiple enrichment/depletion events ~405-385 mm, a period of overall enrichment (Figure 3.4 D). Between ~331 mm and ~320 mm, all records show an overall depletion event (Figure 3.4 E). Both stalagmite calcite $\delta^{18}O$ and $\delta^{13}C$ records reveal a corresponding depletion event at ~320-315 mm and ~300-290 mm (Figure 3.4 F-G). Stalagmite calcite $\delta^{13}C$ and trace metal records show a period of enrichment from ~260-225 mm (Figure 3.4 H), a period of depletion from ~150-125 mm and ~145-132 mm (Figure 3.4 K,N). All records demonstrate episodes of enrichment from ~210-198 mm (Figure 3.4 I); episodes of depletion from ~165-150 mm, ~120-110 mm (Figure 3.4 J, L); and corresponding enrichment/depletion episodes from ~70-57 mm (Figure 3.4 M). Stalagmite $\delta^{13}C$ and trace metal records illustrate a period of enrichment to depletion from ~45-30 mm (Figure 3.4 N). Lastly, from ~5 mm to the end of the stalagmite BCC-025 growth (0 mm), $\delta^{18}O$ and $\delta^{13}C$ records show a corresponding period of depletion (Figure 3.4 O).

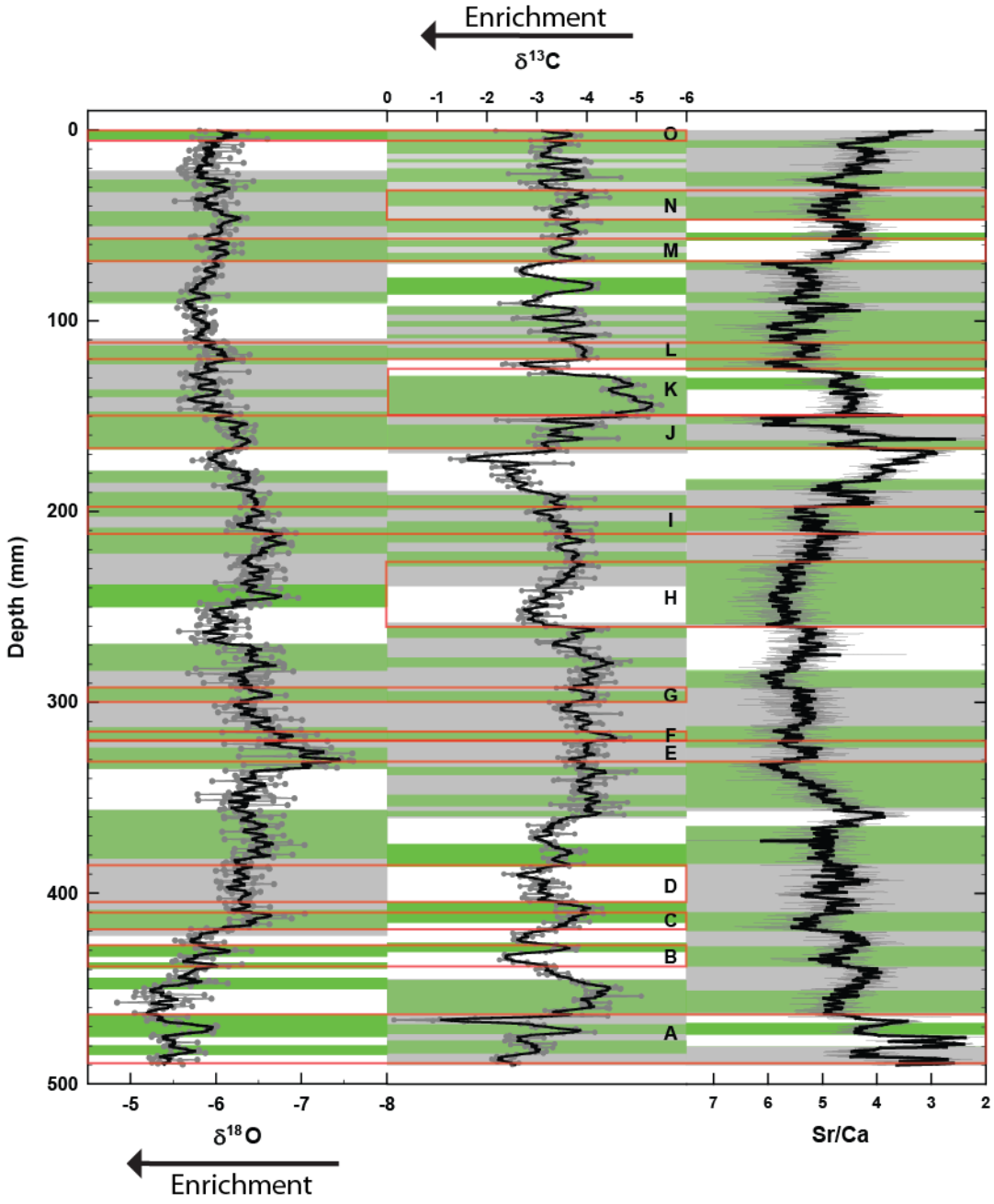

Figure 3.4 Integration of previously defined enrichment/depletion patterns in $\delta^{18}O$, $\delta^{13}C$, and Sr/Ca of BCC-025 outlined in red and labeled by letter for reference.

CHAPTER 4

DISCUSSION

4.1 Age Correlation

Chronological control in past climate reconstruction is of vital importance. Because stalagmite BCC-025 only has two constraining dates, top and bottom, a linear age model must first be constructed. Stalagmite BCC-025 calcite growth began ~628,321 years ago and stopped ~488,777 years ago, recording ~139,544 years of climate in 490 mm of stalagmite calcite. Using this s-point are model, each millimeter in stalagmite BCC-025 represents ~284 years of speleothem growth. The imprecise age determinations of BCC-025, along with multiple hiatuses, represent severe impediments for the reconstruction of a robust time scale of growth. At first glance, approximately ten additional intervals along the growth axis are recommended for further age-dating (Figure 4.1); areas were chosen because they represent the timing of pronounced geochemical/isotopic change in the record.

4.1.1. Visible Growth Hiatuses

Stalagmite BCC-025 visually exhibits seven growth hiatuses of unknown duration that are also observed in the proxy results (Figure 2.1). Age-depth relationships for the hiatuses are approximated using the linear age model. The hiatus at ~536 kyrBP that is visually observed at 165 mm is also resolved in the $\delta^{18}O$ (decrease), $\delta^{13}C$ (decrease), and Sr/Ca results (increase) (Figure 4.2 A). The hiatus at ~542 kyrBP, visually at 187 mm, is marked by a decrease in all results (Figure 4.2 B). The hiatuses observed at 253 mm, 348 mm, 410 mm, and 448 mm are resolved at ~563, ~592, ~608 and ~617 kyrBP, respectively, as increases in all results (Figure 4.2 C-F). Conversely, the hiatus observed near 464 mm is resolved at ~622 kyrBP as a decrease in all results (Figure 4.2 G). A hiatus in stalagmite growth is caused either by a variety

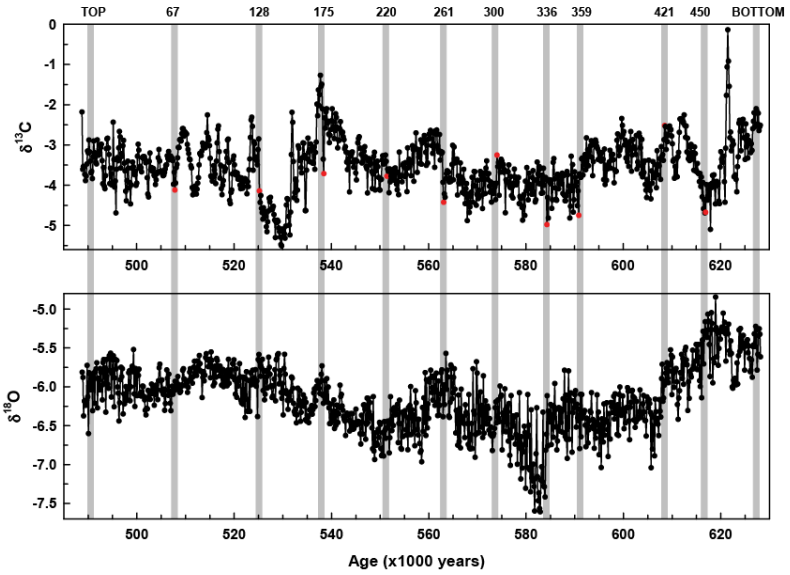

Figure 4.1 Combination plot of $\delta^{18}O$ and $\delta^{13}C$ showing various samples throughout stalagmite BCC-025 that are suggested for further age-dating.

of regional climatic events, such as the cave flooding, freezing or drying out (drought), or due to a localized change in the cave hydrology. The individual causes of growth interruptions in stalagmite BCC-025 are unclear, and may be the result of several factors. If additional speleothems of the same age were found in BCC that continuously grew during BCC-025 hiatuses, it would suggest that the interruptions in growth were caused by local effects, such as an interruption of drip-water above BCC-025.

4.1.2. Marine Isotope Stage Boundaries

A two-point (linear) age model of stalagmite BCC-025 is not sufficiently robust to use for a comparison to other contemporaneous oxygen isotope records (e.g., marine and ice-core records); thus, modification and evaluation of additional tie-points derived from other studies is required. Bradley (1999) gathered the most widely used ages for marine isotope stage (MIS) boundaries from various sources, including a) estimates by linear interpolation from core V28-238, using a mean sedimentation rate of 1.7 cm/10^3 years (Shackleton and Opdyke, 1973) (Table 4.1 A), b) estimates based on the assumption that variations in obliquity have resulted in

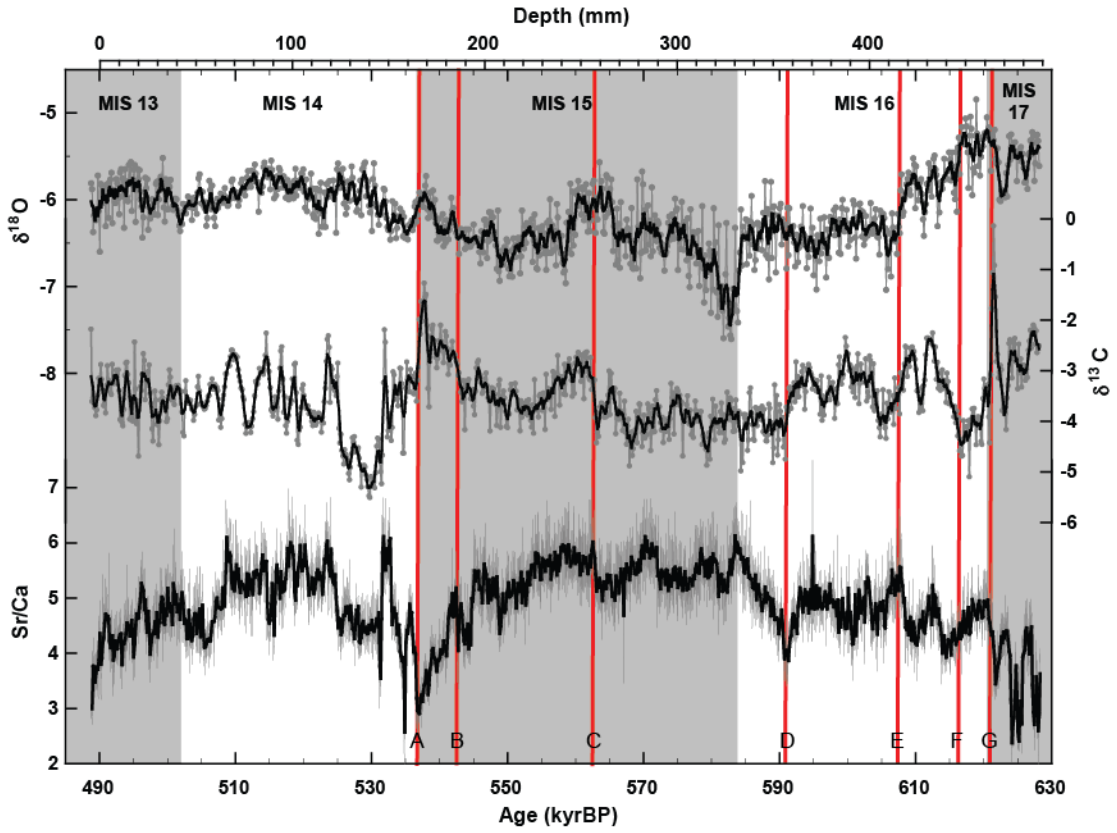

Figure 4.2 Linear age model of stalagmite BCC-025 $\delta^{18}O$, $\delta^{13}C$, and Sr/Ca records. Marine isotope stages illustrated, gray bars representing interglacials, white bars representing glacials. Red lines (A-G) representing visual growth hiatuses.

variations of global ice volume, and that the phase shift between the Earth's tilt and the 41 kyr component of the isotopic record has remained fixed with time (Hays et al., 1976; Kominz et al., 1979; Pisias and Moore, 1981) (Table 4.1 B). Williams et al. (1988) correlated oxygen isotope records from various ocean basins using nannofossil biostratigraphy and paleomagnetic stratigraphy. Spectral analysis of the oxygen isotope signal and comparisons of the signal with the periodicities of the Milankovitch orbital parameters have resulted in a refinement of the absolute age assignments of the late Pleistocene MIS boundaries (Table 4.1 C). Stalagmite BCC-025 $\delta^{18}O$ signatures were correlated with the $\delta^{18}O$ signatures illustrated in Williams et al. (1988), Bassinot et al. (1994), Wright (2000), and Alonso-Garcia et al. (2011) for a visually

refined age model (Figure 4.2). MIS boundary ages from the above mentioned sources were averaged to produce a numerically refined age model for BCC-025 (Table 4.1).

Table 4.1 MIS Boundary Age Estimates

MIS	Estimated Ages (x 10^3 years)					
	A		B	C	Average	D
13/14	502	500	505	521	507	533
14/15	542	551	517	544	539	563
15/16	592	619	579	589	595	621
16/17	627	649	608	622	627	676

Lisiecki and Raymo (2005) present a stack of benthic $\delta^{18}O$ records from 57 globally distributed sites, as well as, a new LR04 age model (Figure 4.3). The LR04 stack contains more variance in benthic $\delta^{18}O$ than previously published stacks of the late Pleistocene as a result of higher-resolution records, improved alignment and tuning, and the abundance of records from the Atlantic. The ages presented by Lisiecki and Raymo (2005) are significantly older than the previous age models, and will be used to represent MIS boundaries in BCC-025 (Table 4.1 D), as illustrated in the final refined age model (Figure 4.4).

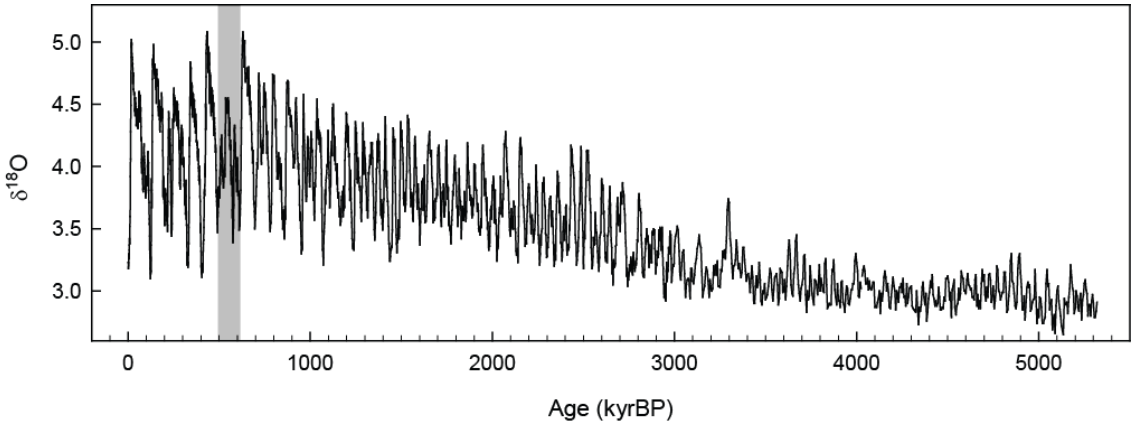

Figure 4.3 LR04 age model (Lisiecki and Raymo, 2005). Gray bar represents time frame of stalagmite BCC-025 record.

4.1.3. Orbital Tuning

Most terrestrial Quaternary paleoclimate work has focused on the last 20 kyrs of Earth history. Orbital variations affect the distribution of radiation from the Sun at the surface of the Earth, and therefore affect the climate. Milankovitch (1941) calculated the changes in seasonal insolation by quantifying the periodic orbital variations in the Earth's obliquity, precession and eccentricity cycles to explain the Quaternary glaciations. Hays et al. (1976) compared climate records from the Southern Ocean with the insolation curves and showed that the climate changes were paced by insolation changes, such that they could be used to explain the cyclic nature of climate change during the past two million years.

Eccentricity (~100 kyr) cycles pace the glacial-interglacial cycles such that it is the lowest frequency component that enables the reoccurrence of low summer insolation maxima. Raymo (1997) suggests that the eccentricity cycle is caused by skipping of higher frequency beats that result in the bundling of either four or five precession cycles. Ridgewell et al. (1999) found that the spectral signature of eccentricity does not appear in the late Pleistocene ice volume record, rather, it shows two distinct peaks near 100 kyrBP and considerable influence near 413 kyrBP. Because of this, the orbital parameters that have primary influence on BCC-025 are obliquity and precession, which control both the spatial and seasonal distribution of incoming solar radiation. However, obliquity (~41 kyr) cycles show little correlation in marine sediment records after 1.4 million years before present (myrBP). The climate response to obliquity appears directly forced with exponentially increasing sensitivity from 5.3-1.4 myrBP, but after 1.4 myrBP the obliquity (41 kyr power) forcing of glacial cycles becomes near constant and uncorrelated (Lisiecki and Raymo, 2007). Precession (~19-23 kyr) cycles exhibit a strong, direct force during the growth period of the stalagmite and strongly relate to changes in eccentricity of the Earth orbit. Figure 4.4 compares the orbital parameters with the $\delta^{18}O$, $\delta^{13}C$, and Sr/Ca records BCC-025, as well as, benthic $\delta^{18}O$ data from Lisiecki and Raymo (2005). At mid Northern Hemisphere latitudes, Raymo (1997) concluded that glacial-interglacial

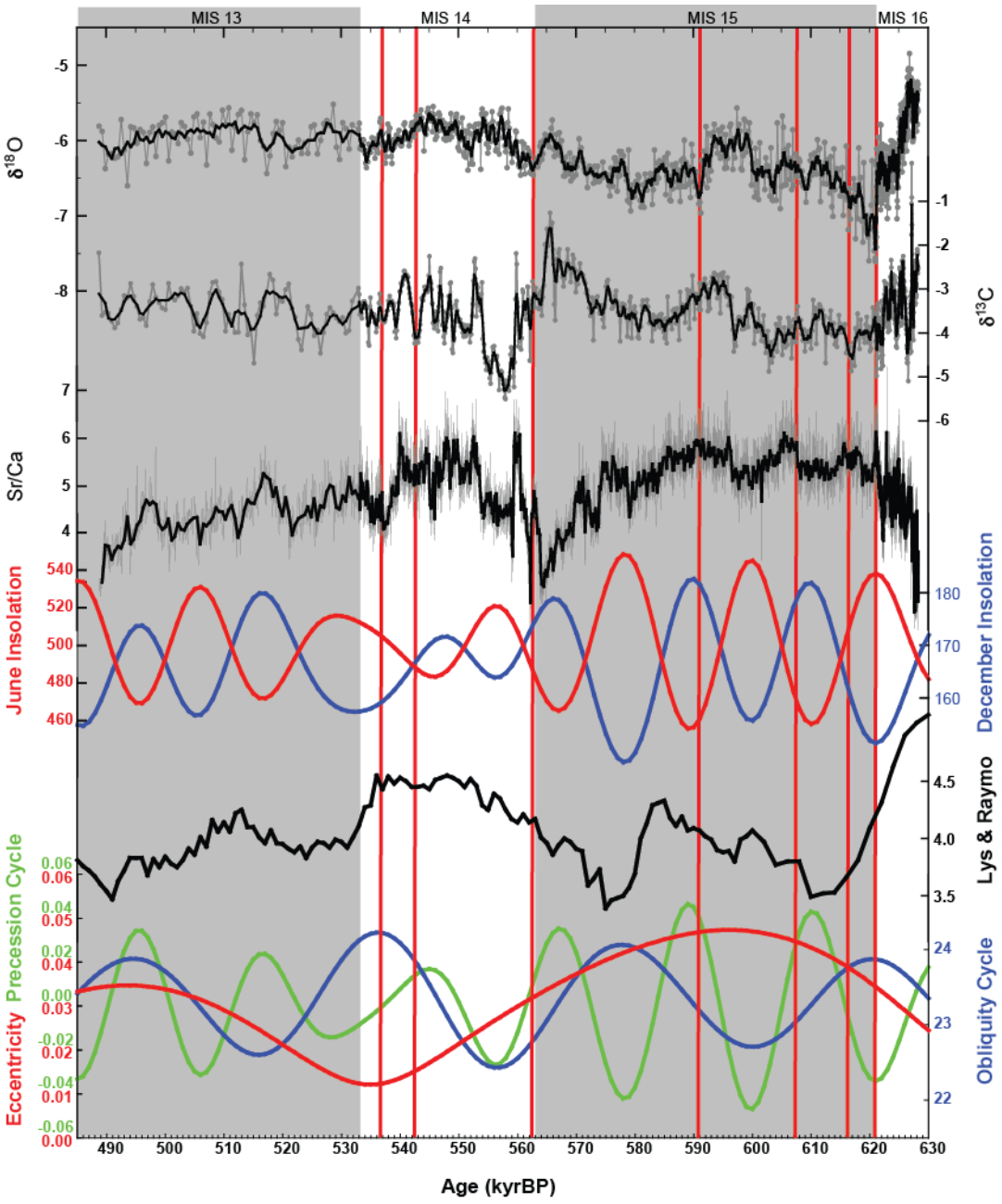

Figure 4.4 Data plotted with enhanced age model that incorporates tie points established from MIS stage boundaries with comparative correlation between BCC-025 $\delta^{18}O$, $\delta^{13}C$, and Sr/Ca records, benthic $\delta^{18}O$ records from Lisiecki and Raymo (2005), June and December insolation at 38°N, and Earth orbital cycles (eccentricity, obliquity, and precession). Red vertical bars represent growth hiatuses in BCC-025. White/gray vertical bars represent glacials/interglacials.

terminations tend to occur after the previous summer insolation maximum was unusually low. If the ice buildup in the Northern Hemisphere is normally limited by the periods of high summer insolation, then the episodic existence of these weak insolation maxima (caused by the superposition of periods of low obliquity and eccentricity) may allow a substantial buildup in Northern Hemisphere ice volume (Ridgewell et al., 1999). The amplitude of precessional cycles and extremes in Northern Hemisphere insolation during MIS 13 and 15 were large, which suggests that the study area responded more strongly to insolation variations, than to interglacial trends in global ice volume. Precession and obliquity are in antiphase, where balancing effects induce weak interglacial intensities.

4.2 Global Proxy Correlation

4.2.1. EPICA Dome C

The EPICA Dome C (EDC) ice-core extends the Vostok ice-core record back to 800 kyrBP, and is the only ice-core covering at least eight glacial cycles. Siegenthaler et al. (2005) conducted a study that compared EDC CO_2 concentrations and δD over six and a half ice age cycles back to 800 kyrBP. It was observed that the coupling of Antarctic temperature and CO_2 did not vary significantly during the past 800 kyr, indicating stable coupling between climate and the carbon cycle during the mid-to-late Pleistocene (Figure 4.5). The CO_2 record from EDC reveals that atmospheric CO_2 variations within glacial-interglacial cycles had a notably different character before and after ~430 kyrBP. Pre-430 kyrBP, the amplitude of temperature swings was lower and the duration of the warm phases were shorter (Siegenthaler et al., 2005).

4.3 Underlying Regional Mechanisms

4.3.1. Vegetation

Regional climate change is evidenced in the speleothem through down axis variations in $\delta^{13}C$. It has been widely accepted that changes in the $\delta^{13}C$ signature reflect changes in above cave vegetation during the deposition of stalagmite calcite, which infiltrates the overlying soil and epikarst. The soil zone is highly significant to stalagmite calcite $\delta^{13}C$; it is where plant roots

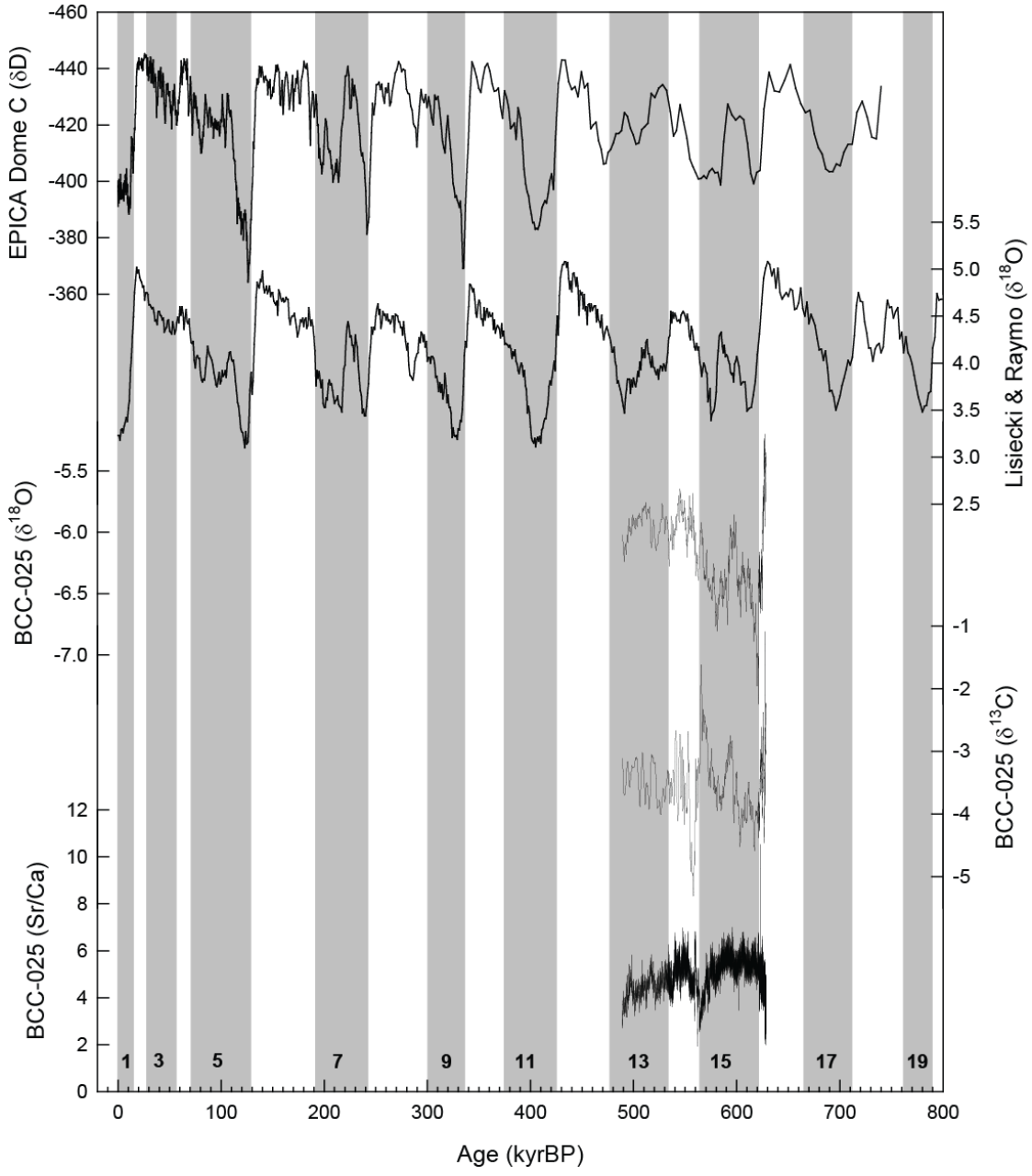

Figure 4.5 Climate data spanning the last 800,000 years including BCC-025 $\delta^{18}O$, $\delta^{13}C$, and Sr/Ca records, Lisiecki and Raymo (2005) $\delta^{18}O$ record, and EPICA Dome C ice-core, δD record (EPICA, 2004).

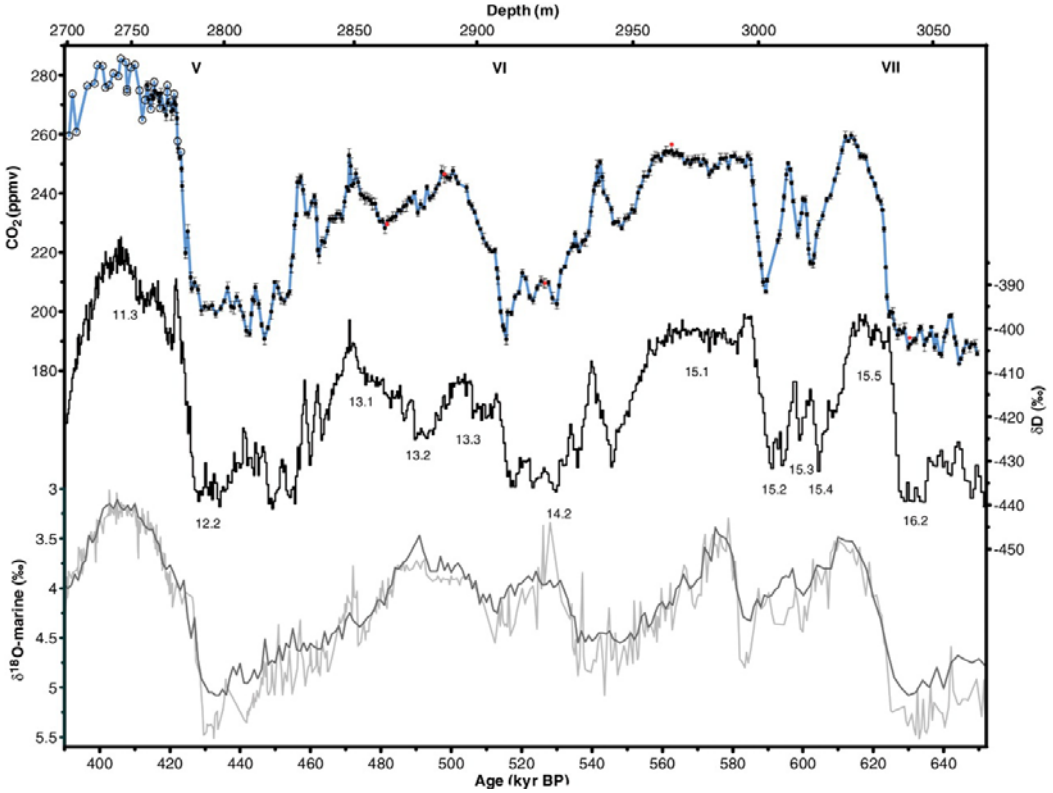

Figure 4.6 EPICA Dome C CO_2 data (EPICA Community Members, 2004), EDC δD data, global benthic $\delta^{18}O$ data (Lisiecki and Raymo, 2005) with approximate MIS (Bassinot et al., 1994) and glacial terminations labeled (Siegenthaler et al., 2005).

respire and microbial respiration occurs, causing the subsequent break down of organic materials (derived from vegetation). It is also widely accepted that other mechanisms governing the stalagmite $\delta^{13}C$ signature are also a function of water residence time in the epikarst zone. Given a long residence time, the $\delta^{13}C$ signature may include carbon signatures of the bedrock material, reflecting more than just vegetation. Fractionation between the stalactite and stalagmite due to evaporation or degassing, as well as, possible degassing of the ground-waters in the epikarst before entering the cave could both increase the calcite $\delta^{13}C$ signature preserved in the speleothem (Baker et al., 1997). Stalagmite BCC-025 does not show any

correlation between $\delta^{18}O$ and $\delta^{13}C$, providing evidence that negligible kinetic fractionation has occurred (Figure 4.6).

Glacial advances reduce the amount of moisture available and thus, reduce the amount of vegetation in the region. After a glacial period, $\delta^{13}C$ values are elevated since photosynthetic pathways were not being utilized, and are now primarily dependent on carbon enriched bedrock leaching. Sr/Ca ratios are in agreement, decreased due to the lack of respiration in the soil zone because of insufficient moisture availability. While temperatures recover after a glacial, so does the vegetation, as can be observed by shifts in the trace element ratio. During this recovery, trace elements vary inversely with $\delta^{13}C$, while $\delta^{18}O$ is increasing. Interglacials are period during which vegetation thrives and stabilizes, assuming moisture is abundant.

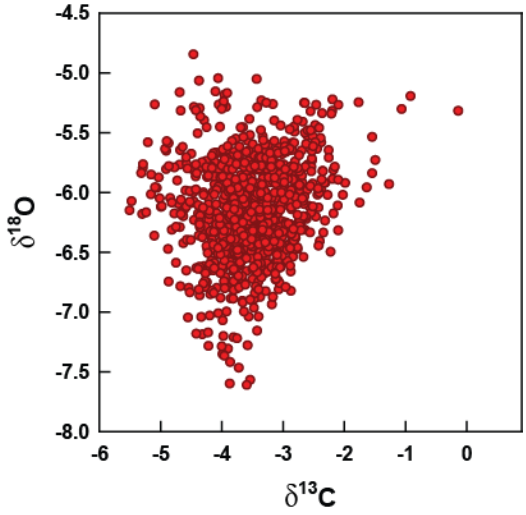

Figure 4.7 Plot of $\delta^{13}C$ *versus* $\delta^{18}O$, demonstrating a lack of correlation, suggesting that negligible kinetic fractionation is taking place in BCC-025.

While many of the variations in soil organic matter $\delta^{13}C$ values have been suggested to be the result of differences in the C_3 and C_4 contributions, there is no evidence that C_4 vegetation existed at the study site during BCC-025 growth. Springer et al. (2008) came to the conclusion that $\delta^{13}C$ values in stalagmite BCC-002 (Holocene age) from the present study area,

pre-2.1 kyrBP, are not affected by C_4 vegetation. Observed changes in $\delta^{13}C$ values are attributable to changes in soil productivity and respiration, but not to major changes in C_3 and C_4 abundances. The absence of pre-Holocene Climatic Optimum data prevents interpretation of vegetation types (Springer et al., 2009).

For purposes of this study, stalagmite $\delta^{13}C$ values can also be interpreted to reflect the abundance of vegetation. Stalagmite $\delta^{13}C$ values are more depleted when climate is relatively moist, due to increased soil respiration, and enriched when climate is dry, due to decreased soil respiration (McDermott, 2004). Trace element signatures (Sr/Ca) are commonly interpreted to reflect change in moisture. When $\delta^{13}C$ and Sr/Ca co-vary, it is interpreted that they are controlled by the same process.

4.4 BCC-025 Climate History

4.4.1. $\delta^{18}O$, $\delta^{13}C$, and Sr/Ca Records of BCC-025

In a previous study of Holocene stalagmite BCC-002, the stalagmite $\delta^{18}O$ signature indicates the balance of summer and/or winter moisture, the seasonality of precipitation (Hardt et al., 2010). The most dominant $\delta^{18}O$ shift occurs during MIS 16 where there is strong summer moisture. This summer moisture is decreasing into strong winter moisture along the MIS 15/16 boundary. Throughout MIS 15, $\delta^{18}O$ increases toward summer time moisture from early to mid MIS 15 and dips to lower summer moisture at the end of MIS 15. A low in the $\delta^{18}O$ signature across 14/15 boundary indicates that the seasonality of precipitation was also low, meaning that there is a decrease in summer precipitation. Throughout MIS 14 there is a relative high in $\delta^{18}O$ reflecting increased summer moisture, continuing through MIS 13, ending in an overall low in the BCC-025 record.

Stalagmite calcite trace metal ratio (Sr/Ca) and $\delta^{13}C$ signature typically indicates shifts in wet/dry conditions, as well as $\delta^{13}C$ indicating biological influence. Two dominant $\delta^{13}C$ peaks occur in BCC-025, the first at the beginning of MIS 16 and another at the end of MIS 14, both glacial periods, where conditions are relatively wet according to Sr/Ca ratio, but depleted in

$\delta^{13}C$. Because $\delta^{13}C$ and Sr/Ca do not covary, $\delta^{13}C$ may indicate more of the biological influence than wet/dry conditions. Throughout the first half of MIS 15, $\delta^{13}C$ is relatively depleted (low), while Sr/Ca is high, indicating that the conditions were mostly dry with an increase in biological activity. In the latter half of MIS 15, toward the MIS 14/15 boundary there is a shift in the records; $\delta^{13}C$ is increasing to the second peak and Sr/Ca is decreasing at a similar rate. This indicates a shift to wet conditions just before the glacial MIS 14. Within MIS 14, the $\delta^{13}C$ signature is at the lowest value, while Sr/Ca ratio is at the highest value. This is another indication of dry conditions, where the $\delta^{13}C$ signature could possibly be illustrating a drastic increase in biologic activity. At this point, with limited proxies available for comparison, the assumption that the $\delta^{13}C$ simply indicates a change in biologic productivity is acceptable. There is not a sudden transition at the MIS 13/14 boundary, indicating that there was a steady progression out of the glacial period. Stalagmite calcite $\delta^{13}C$ signature remains relatively constant on average, and Sr/Ca ratio shows a decreasing trend through the remainder of the record. With the increase in summer moisture through MIS 13, as indicated by the $\delta^{18}O$ record, Sr/Ca also reflects an increase in wet conditions.

CHAPTER 5

CONCLUSION

The purpose of the present study was to attempt to provide an initial evaluation of climate changes that occurred across the interval of MIS 13 back through MIS 16 or 17, depending on the age correlation used. The uniqueness of this study is that it is neither from marine nor ice-core records, and instead, comes from the mid-latitudes of eastern North America. The value of the study, despite inherent weaknesses in the age chronology, is that it demonstrates paleoclimate variability during a time period when humans did not exist, but where heavily populated centers now exist. Furthermore, despite the limitations of age-dating, the results presented in this study can be utilized by climate scientists to infer the boundaries of climate change, and perhaps the relative importance of various climate drivers during the early-Late Pleistocene.

Because of the flawed nature of the current age chronology, it is difficult to accurately and precisely define the glacial/interglacial shifts that are undoubtedly preserved in the record. This is particularly the case due to the lessened glacial/interglacial variability, when compared to the Late Pleistocene swings (Figure 4.4). Notably, the glaciations of the early Late Pleistocene are apparently equal in magnitude to those in the Late Pleistocene, however, the interglacials are much less pronounced. Thus, the present record is not as punctuated as records of the younger glacial/interglacial episodes.

What can be gleaned from the data set is that changes is $\delta^{18}O$ do not coincide with changes in $\delta^{13}C$ and Sr/Ca. This suggests, based on previous evidence, that the long-term seasonality of precipitation is not affected by the same factors that govern $\delta^{13}C$ and Sr/Ca (Springer et al., 2008; Hardt et al., 2010). Another observation is that the $\delta^{13}C$ and Sr/Ca are not

intimately linked throughout most of the record, suggesting that the factors driving each proxy are not closely related. The lack of covariation is in direct contradiction to a previous study, which hypothesized that both proxies were heavily influenced by the long-term cycle of precipitation (wet/dry cycles) (Springer et al., 2008). At present the lack of covariability between these two proxies is hypothesized to represent a general lack of importance in the precipitation history, an in increase in other influences, such as, biological activity, and related processes.

Based on an age chronology developed by integrating previously defined MIS boundaries with the bounding 230Th ages, a temporal context was established for stalagmite BCC-025 (Figure 4.4).

As a final note, the study demonstrates that further studies should place more emphasis on developing geochronological constraints. A climate record is only as good as its age model. It is anticipated that better age constraints will be generated shortly.

REFERENCES

Alley, R.B., Gow, A.J., Johnsen, S.J., Kipfstuhl, J., Meese, D.A., Thorsteinsson, T., 1995. Comparison of deep ice cores. *Nature*, 373; 393-394.

Alley, R.B., Mayewski, P.A., Sowers, T., Stuiver, M., Taylor, K.C., Clark, P.U., 1997. Holocene climatic instability: A prominent, widespread event 8200 years age. *Geology*, 25(6); 483-486.

Alley, R.B., 2000. Ice-core evidence of abrupt climate changes. *PNAS*, 97(4); 1331-1334.

Alonso-Garcia, M., Sierro, F.J., Flores, J.A., 2011. Arctic front shifts in the subpolar North Atlantic during the Mid-Pleistocene (800-400 ka) and their implications for ocean circulation. *Palaeogeography, Palaeoclimatology, Palaeoecology*, doi: 10.1016/j.paleo.2011.09.004.

Asmerom, Y., Polyak, C.J., Stephen J.B., 2010. Variable winter moisture in the southwestern United States linked to rapid glacial climate shifts. *Nature Geoscience*; doi: 10.1038/NGEO754

Baker, A., Ito, E., Smart, P. L., McEwan, R. F., 1997. Elevated and variable values of 13C in speleothems in a British cave system. *Chemical Geology*, 136; 263-270.

Baker, R.G., Gonzalez, L.A, Raymo, M., Bettis III, E.A., Reagan, M.K., and Dorale, J.A., 1998. Comparison of multiple proxy records of Holocene environments in Midwestern USA. *Geology*, 26(12); 1131-1134.

Bar-Matthews M., Ayalon A., Kaufman A., Wasserburg G.J., 1999. The Eastern Mediterranean paleoclimate as a reflection of regional events: Soreq Cave, Israel. *Earth and Planetary Science Letters,* 166; 85-95.

Bassinot, F.C., Labeyrie, L.D., Vincent, E., Quidelleur, X., Shackleton, N.J., Lancelot, Y., 1994. The astronomical theory of climate and the age of the Brunhes-Matuyama magnetic reversal. *Earth and Planetary Science Letters*, 126; 91-108.

Becquey, S., Gersonde, R., 2002. Past hydrographic and climatic changes in the Subantarctic Zone of the South Atlantic – The Pleistocene record from ODP Site 1090. *Palaeogeography, Palaeoclimatology, Palaeoecology*, 182(3-4); 221-239.

Berger, A., 1988. Milankovitch Theory and Climate*. Review of Geophysics*, 26; 624-657.

Berger, A., Loutre, M.F., 1994. Precession, eccentricity, obliquity, insolation and paleoclimates. NATO ASI Series, I22; 107-151.

Berger, W.H., 1990. The Younger Dryas cold spell, a quest for causes. Global and Planetary Change, 3 (3); 219-237, Doi:10.1016/0921-8181(90)90018-8.

Biscaye, P.E., Grousset, F.E., Revel, M., Van der Gaast, S., Zielinski, G.A., Vaars, A., Kukla, G., 1997. Asian provenance of glacial dust (stage 2) in the Greenland Ice Sheet Project 2 ice core, Summit, Greenland. *Journal of Geophysical Research*, 102(C12); 26765-26781, doi:10.1029/97JC01249.

Bond, G.C., Kromer, B., Beer, J., Muscheler, R., Evans, M., Showers, W., Hoffmann, S., Lotti-Bond, R., Hajdas, I., Bonani, G., 2001. Persistent solar influence on North Atlantic climate during the Holocene. *Science*, 294; 2130-2136.

Bradley, R.S., 1999. Paleoclimatology: Reconstructing Climates of the Quaternary. Academic Press, San Diego, 610pp.

Broecker, W.S., 1963. A Preliminary Evaluation of Uranium Series Inequilibrium as a Tool for Absolute Age Measurement on Marine Carbonates, *Journal of. Geophysical Research*, 68(9); 2817–2834, doi:10.1029/JZ068i009p02817.

Broecker, W.S., 1994. Massive iceberg discharges as triggers for global climate change. *Nature*, 372; 421-424.

Brook, E.J., 2005. Tiny bubbles tell all. Science, 310; 1285-1287.

Buckles, J., Rowe, H., Gao, Y., Cheng, H., Edwards, R.L., Springer, G., Hardt, B., 2011. A novel method for trace elemental analysis of speleothems using μ-XRF. Geological Society of America Abstracts with Programs, 43 (5); 588.

Candy, I., Coope, G.R., Lee, J.R., Parfitt, S.A., Preece, R.C., Rose, J., Schreve, D.C., 2010. Pronounced warmth during early Middle Pleistocene interglacials: Investigating the Mid-Brunhes Event in the British terrestrial sequence. Earth Science Reviews, doi:10.1016/j.earscirev.2010.09.007.

Chapellaz, J., Blunier, T., Raynaud, D., Barnola, J. M., Schwander, J., and Stauffer, B., 1993. Synchronous changes in atmospheric CH4 and Greenland climate between 40 and 8 kyr ago. *Nature*, 366; 443-445

Cheng, H., Edwards, L., Broecker, W.S., Denton, G.H., Kong, X., Want, Y., Zhang, R., Wang, X., 2009. Ice age terminations. *Science*, 326; 248-252.

Cheng, H., Fleitmann, D., Edwards, R.L., Wang, X., Cruz, F.W., Auler, A.S., Mangini, A., Wang, Y., Kong, X., Burns, S.J., Matter, A., 2009. Timing and structure of the 8.2 kyr B.P. event inferred from $\delta^{18}O$ records of stalagmites from China, Oman, and Brazil. *Geology*, 37(11); 1007-1010.

Clark, I. D., Fritz, P., 1997. Environmental isotopes in hydrogeology. CRC Press/Lewis Publishers, Boca Raton, FL; 328 pp.

Cosford, J., Qing, H., Eglington, B., Mattey, D., Yuan, D., Zhang, M., Cheng, H., 2008. East Asian monsoon variability since the Mid-Holocene recorded in a high-resolution, absolute-dated aragonite speleothem from eastern China. *Earth and Planetary Science Letters*, 275; 296-307.

Cruz, F.W., Karmann, I., Viania, O., Burns, S.J., Ferrari, J.A., Vuille, M., Sial, A.N., Moreira, M.Z., 2005. Stable isotope study of cave percolation waters in subtropical Brazil: Implications for paleoclimate inferences from speleothems. *Chemical Geology*, 220; 245–262.

Dansgaard, W., 1964. Stable Isotopes in precipitation. *Tellus*, 16; 436-468.

Dasher, G.R., Balfour, W.M., 1994. The caves and karst of the Buckeye Creek Basin. *West Virginia Speleological Society Bulletin*, 12; West Virginia Speleological Society, Barracksville, WV, 238 pp.

Dean, W.E., Piper, D.Z., and Arthur, M.A., 1995, Accumulation of Mo in Cariaco Basin Sediments: A record of paleoceanographic change during the last 20,000 years: American Geophysical Union Fall Meeting, EOS.

DeAngelis, M., Barkov, N.I., Petrov, V.N., 1987. Aerosol concentrations over the last climatic cycle (160 kyr) from an Antarctic ice core. *Nature*, 325; 318-321.

Denniston, R.F., Asmerom, Y., Polyak, V., Dorale, J.A., Carpenter, S.J., Trodick, C., Hoye, B., Gonzalez, L.A., 2007. Synchronous millennial-scale climatic changes in the Great Basin and the North Atlantic during the last interglacial. *Geology*, 35(7); 619-622.

Dorale, J.A., Gonzalez, L.A., Reagan, M.K., Picket, D.A., Murrell, M.T., Baker, R.G., 1992. A high-resolution record of Holocene climate change in speleothem calcite from Cold Water Cave, northeast Iowa. Science, 258; 1626-1630, doi: 10.1126/science.258.5088.1626.

Dorale, J.A., Edwards, R.L., Ito, E., González, L.A., 1998. Climate and vegetation history of the midcontinent from 75 to 25 ka: A speleothem record from Crevice Cave, Missouri, USA. *Science*, 282; 1871-1873.

Dykoski, C.A., Edwards, R.L., Cheng, H., Yuan, D., Cai, Y., Zhang, M., Lin, Y., Qing, J., An, Z., Revenaugh, J., 2005. A high resolution, absolute-dated Holocene and deglacial Asian monsoon record from Dongge Cave, China. *Earth and Planetary Science Letters,* 233; 71-86.

Enfield, D.B., Mestas-Nuñez, A.M., Trimble, P.J., 2001. The Atlantic multidecadal oscillation and its relation to rainfall and river flows in the continental U.S.. *Geophysical Research Letters*, 28(10); 2077-2080.

Edwards, R.L. Chen J.H. Wasserburg G.J., 1987. ^{238}U- ^{234}U- ^{230}Th- ^{232}Th systematics and the precise measurements of time over the past 500,000 years. *Earth and Planetary Science Letters*, 81; 175-192.

EPICA Community Members, 2004. Eight glacial cycles from an Antarctic ice core. *Nature*, 249; 623-628.

Fairchild, I.J., Treble, P.C., 2009. Trace elements in speleothems as recorders of environmental change. *Quaternary Science Review*, 28; 449-468, doi:10.1016/j.quascirev.2008.11.007.

Fairchild, I.J., Borsato, A., Tooth, A.F., Frisia, S., Hawkesworth, C.J., Huang, Y., McDermott, F., Spiro, B., 2000. Controls on trace element (Sr-Mg) compositions of carbonate cave waters: implications for speleothem climatic records. *Chemical Geology*, 166; 255-269.

Fairchild, I.J., Baker, A., Borsato, A., Frisia, S., Hinton, R. W., McDermott, F., Tooth, A. F., 2001. Annual to sub-annual resolution of multiple trace-element trends in speleothems. *Journal of the Geological Society*, 158; 831-841, doi:10.1144/jgs.158.5.831.

Fairchild, I.J., Smith, C.J., Baker, A., Fuller, L., Spötl, C., Mattey, D., McDermott, F., E.I.M.F., 2006. Modification and preservation of environmental signals in speleothems. *Earth-Science Reviews,* 75; 105-153.

Fairchild, I.J., Frisia, S., Borsato, A., Tooth, A.F., 2007. Speleothems, in: Geochemical sediments and landscapes (ed. Nash, D. J. and McLaren, S. J.). Blackwells, Oxford, UK. ISBN 1405121595.

Fleitmann, D., Burns, S.J., Mudelsee, M., Neff, U., Kramers, J., Mangini, A., Matter, A., 2003. Changing moisture source over the last 330,000 years in Northern Oman from fluid-inclusion evidence in speleothems. *Quart. Research*, 60; 223–232.

Frappier, A., Sahagian, D., González, L. A., and Carpenter, S. J., 2002, El Niño events recorded by stalagmite carbon isotopes. Science, 298, 565.

Friedman, I., Smith, G., 1970. Deuterium content of snow cores from Sierra Nevada area. *Science*, 169; 467-470.

Friedman, I., O'Neil J.R., 1977. Compilation of stable isotope fractionation factors of geochemical interest. In: Fleischer M. (Ed.), *Data of Geochemistry:: U.S. Geological Survey Professional Paper 440-K,* Washington, 12 p.

Garnett, E.R., Andrews, J.E., Preece, R.C., Dennis, P.F., 2004. Climatic change recorded by stable isotopes and trace elements in a British Holocene tufa. *Journal of Quaternary Science*, 19(3); 251-262.

Gat, J.R., 1983. Precipitation, groundwater, and surface waters: Control of climate parameters and their utilization as palaeoclimatic tools. In: Palaeoclimates and Palaeowaters: a Collection of Environmental Isotope Studies. IAEA, Vienna; 3-12.

Genty, D., Vokal B., Obelic B., Massault M., 1998. Bomb 14C time history recorded in two modern stalagmites; importance for soil organic matter dynamics and bomb 14C distribution over continents. Earth and Planetary Science Letters, 160(3); 795-809.

Genty, D., Blamart D., Ouahdi R., Gilmour M., Baker A., Jouzel A., and Van-Exter S., 2003: Precise dating of Dansgaard–Oeschger climate oscillations in western Europe from stalagmite data. Nature, 421; 833-837.

Grootes, P.M., Stuiver, M., White, J.W.C., Johnsen, S., Jouzel, J., 1993. Comparison of oxygen isotope records from the GISP2 and GRIP Greenland ice cores. *Nature*, 366; 552-554.

Hardt, B., Rowe, H.D., Springer, G.S., Cheng, H., Edwards, R.L., 2010. The seasonality of east ventral North American precipitation based on three coeval Holocene speleothems from southern West Virginia. *Earth and Planetary Science Letters*, 295; 342-348.

Haug, G. H., Hughen, K.A., Sigman, D. M., Peterson, L. C., Röhl, U., 2001. Southward Migration of the Intertropical Convergence Zone through the Holocene. *Science*, v. 293; 1304-1308.

Hays, J.D., Imbrie, J., Shackelton, N.J., 1976. Variations in the Earth's orbit: pacemaker of the ice ages. *Science*, 194; 1121-1132.

Hendy, H.C., 1971. The isotopic geochemistry of speleothems, I. The calculation of the effects of different modes of formation on the isotopic composition of speleothems and their applicability as paleoclimate indicators. *Geochem. Cosmochem. Acta,* 35; 801-824.

Higgins, P., MacFadden, B.J., 2004. "Amount Effect" recorded in oxygen isotopes of Late Glacial horse (Equus) and bison (Bison) teeth from the Sonoran and Chihuahuan deserts, southwestern United States. *Palaeogeography, Palaeoclimatology, Palaeoecology*, 206; 337-353, doi: 10.1016/j.palaeo.2004.01.011.

Hill, C.A., Forti, P., 1997. Cave Minerals of the World (2nd ed.). *National Speleological Society Huntsville*; 464 pp.

Houghton, J.T., Ding Y., Griggs D.J., Noguer M., Van Der Linden P.J., Dai X., Maskell K., Johnson C.A. (Editors), 2001: Climate Change 2001: The Scientific Basis, Contribution of Working Group 1 to the Third Assessment Report of the Intergovernmental Panel on Climate Change, Cambridge University Press, Cambridge; 892p.

Huang, Y., Fairchild, I.J., Borsato, A., Frisia, S., Cassidy, N. J., McDermott, F., Hawkesworth, C.J., 2001. Seasonal variations in Sr, Mg, and P in modern speleothems (Grotta di Ernesto, Italy). *Chemical Geology*, 175; 429-448.

Hughen, K.A., Overpeck, J.T., Peterson, L.C. Trumbore, S., 1996, Rapid climate changes in the tropical Atlantic region during the last deglaciation. *Nature*, 380; 51-54.

Hughen, K.A., Eglinton, T., Xu, L., Makou, M., 2004. Abrupt tropical vegetation response to rapid climate changes. *Science*, 304; 1955-1959.

Huybers, P., 2007. Glacial variability over the last two million years: an extended depth-derived agemodel, continuous obliquity pacing, and Pleistocene progression. *Quaternary Science Reviews*, 26; 37-55.

Ingraham, N.L., 1998. Isotopic variations in precipitation. In: Kendall, C., McDonnell, J. (Eds.), Isotope Tracers in Catchment Hydrology. Elsevier, Amsterdam, 87–118 pp.

Johnson, K.R., Hu, C.Y, Belshaw, N.S., Henderson, G.M., 2006. Seasonal trace-element and stable-isotope variations in a Chinese speleothem: The potential for high-resolution paleomonsoon reconstruction. *Earth and Planetary Science Letters*, 244; 394-407.

Jones, P.D., Osborn, T.J., Briffa, K.R., 2001. The evolution of climate over the last millennium. *Science*, 292; 662-667.

Jones, P.D., Mann, M.E., 2004. Climate over past millennia. *Reviews of Geophysics*, 42; 2003RG000143.

Jouzel, J., Masson-Delmotte, V., Cattani, O., Dreyfus, G., Falourd, S., Hoffmann, G., Minister, B., Nouet, J., Barnola, J.M., Chappellaz, J., Fischer, H., Gallet, J.C., Johnsen, S., Schilt, A., Schwander, J., Selmo, E., Souchez, R., Spahni, R., Stauffer, B., Steffensen, J.P., Stenni, B., Stocker, T.F., Tison, J.L., Werner, M., Wolff, E.W., 2007. Orbital and millennial Antarctic climate varianility over the Past 800,000 years. *Science*, 317; 793-796.

Kaufmann, G., Dreybrodt, W., 2004. Stalagmite growth and palaeoclimate: an inverse approach. *Earth and Planetary Science Letters*, 224; 529-545.

Kobashi, T., Severinghaus, J.P., Brook, E.J., Barnola, J., Grachev, A.M., 2007. Precise timing and characterization of abrupt climate change 8,200 years ago from air trapped in polar ice. *Quarternary Secience Reviews*, 26; 1212-1222.

Kominz, M.A., Heath, G.R., Ku, T.L., Pisias, N.G., 1979. Brunhes time scales and the interpretation of climatic change. *Earth and Planetary Science Letters*, 45; 394-410.

Lachniet, M.S., 2009. Climatic and environmental controls on speleothem oxygen-isotope values, *Quaternary Science Reviews*, 28; 412-432.

Lambert, F., Delmonte, B., Petit, J.R., Bigler, M., Kaufmann, P.R., Hutterli, M.A., Stocker, T.F., Ruth, U., Steffensen, J.P., Maggi, V., 2008. Dust-climate couplings over the past 800,000 years from the EPICA Dome C ice core. *Nature*, 452 (7187); 616-619.

Lauritzen, S.E., 2003. Reconstructing Holocene climate records from speleothems. In: Global Change in the Holocene; 242-263. Mackay, A., Battarbee, R., Birks, J., Oldfield, F. (eds.). Arnold, London.

Lea, D.W., Pak, D.K., Peterson, L.C.,Hughen, K.A., 2003. Synchroneity of Tropical and High-Latitude Atlantic Temperatures over the Last Glacial Termination. *Science*, 301 (5638); 1361-1364.

Legrand, M., Mayewski, P.A., 1997. Glaciochemistry of poar ice cores: a review. *Reviews of Geophysics*, 35; 219-243.

Lisiecki, L.E., Raymo, M.E., 2005. A Pliocene-Pleistocene stack of 57 globally distributed bethic $\delta^{18}O$ records. *Paleooceanography*, 20; doi:10.1029/2004PA001071.

Lisiecki, L.E., Raymo, M.E., 2007. Plio-Pleistocene climate evolutionL Trends and transitions in glacial cycle dynamics. *Quaternary Science Reviews*, 26; 56-69.

LoDico, J.M., Flower, B.P., Quinn, T.M., 2006. Subcentennial-scale climatic and hydrologic variability in the Gulf of Mexico during the early Holocene. Paleooceanography, 21; PA3015, doi:10.1029/2005PA001243.

Lundberg, J., Lord, T.C., Murphy, P.J., 2010. Thermal ionization mass spectrometer U-Th dates on Pleistocene speleothems from Victoria Cave, North Yorkshire, UK: Implications for paleoenvironment and stratigraphy over multiple glacial cycles. *Geosphere*, 6; 379-395.

Mann, M.E., 2001. Climate during the past millennium. *Weather*, 56; 91-101.

McCabe, G. J., M. A. Palecki, and J. L. Betancourt (2004), Pacific and Atlantic Ocean influences on multidecadal drought frequency in the United States. *Proc. Natl. Acad. Sci. U.S.A*., 101; 4136–4141, doi:10.1073/pnas.0306738101.

McDermott, F., 2004. Palaeo-climate reconstruction from stable isotope variations in speleothems: a review. *Quaternary Science Reviews*, 23; 901-908.

McDermott, F., Frisia, S., Huang, Y., Longinelli, A., Spiro, B., Heaton, T.H.E., Hawkesworth, C.J., Borsato, A., Keppens, E., Fairchild, I. J., Van Der Borg, K., Verheyden, S., Selmo, E., 1999. Holocene climate variability in Europe: evidence from δ18O and textural variations in speleothems. *Quaternary Science Reviews*, 18; 1021-1038.

Meese, D.A., Alley, R.B., Gow, A.J., Grootes, P.M., Mayewski, P.A., Ran, M., Taylor, K.C., Waddington, E.D., Zielinski, G.A., Bond, G.C., 1994. Preliminary depth-age scale of the GISP2 ice core. *CRREL Spec. Rep*. 94-1; 66 pp., Cold Reg. Res. and Eng. Lab., Hanover, N.H., 1994.

Mickler, P.J., Banner, J.L., Stern, L., Asmerom, Y., Edwards, R.L., Ito, E., 2004. Stable isotope variations in modern tropical speleothems: Evaluating equilibrium vs. kinetic isotope effects. *Geochimica et Cosmochimica Acta*, 68(21); 4381-4393.

Mickler, P.J., Stern, L.A., Banner, J.L., 2006. Large kinetic isotope effects in modern speleothems. *GSA Bulletin*, 118(1/2); 65-81.

Milankovitch, M., 1941. Kanon der Erdbestrahlung und seine Andwendung auf das Eiszeiten-problem. Royal Serbian Academy, Belgrade.

Mitchell, J.F.B, Grahame, N.S., Needham, K.J., 1988. Climate simulations for 9000 years before present: Seasonal variations and effect of the Laurentide Ice Sheet, Journal of Geophysical Research, 93; 8283-8303.

Montero, M.E., Aspiazu, J., Pajón, J., Miranda, S., Moreno, E., 2000. PIXE study of Cuban quaternary Paleoclimate geological samples and speleothems. *Applied Radiation and Isotopes*, 52; 289-297.

Mook, W.G., 2006. Introduction to Isotope Hydrology: Stable and Radioactive isotopes of Hydrogen, Oxygen and Carbon. Taylor & Francis Group. London, Great Britain, 226 p.

Moore, G.W. and Sullivan, G.N., 1978. The study of caves. *Speleology*; 150 pp.

Morse, J.W., Arvidson, R.S., 2002. The dissolution kinetics of major sedimentary carbonate minerals. *Earth Science Reviews*, 58; 51-84.

Motyka, J., Gradziński, M., Bella, P., Holúbek, P., 2005. Chemistry of water from selected caves in Slovakia-a reconnaissance study. *Environmental Geology*, 48(6); 682-692.

Muscheler, R., Kromer, B., Björck, S., Svensson, A., Friedrich, M., Kaiser, K.F., Southon, J., 2008. Tree rings and ice cores reveal ^{14}C calibration undertainities during the Younger Dryas. *Nature Geoscience*, 1; 263-267.

Musgrove M., Banner J. L., Mack L. E., Combs D. M., James E. W., Cheng H., Edwards R. L., 2001. Geochronology of late Pleistocene to Holocene speleothems from central Texas: Implications for regional paleoclimate. *GSA Bulletin*, 113; 1532–1543.

Musgrove, M., Banner, J.L., 2004. Controls on the spatial and temporal variability of vadose drip water geochemistry: Edwards Aquifer, central Texas. *Geochim. Cosmochim. Acta*, 68; 1007-1020, doi:10.1016/j.gca.2003.08.014.

Neff, U., Burns, S. J., Mangini, A., Mudelsee, M., Fleitmann, D., Matter, A., 2001. Strong coherence between solar variability and the monsoon in Oman between 9 and 6 hyr ago. *Nature*, 411, 290-293.

O'Leary, M.H., 1988. Carbon isotopes in photosynthesis. *Bioscience*, 38; 325-326.

O'Neil, J.R., Epstein, S., 1966. Oxygen isotope fractionation in the system dolomite-calcite-carbon dioxide. *Science*, 152; 198-201.

Palmer, A.N., 2002. Cave Geology. Cavebooks, Dayton, Ohio; 454p.

Pandolfi, J.M., 1996. Limited membership in Pleistocene reed coral assemblages from the Huon Peninsula, Papua New Guinea: Constancy during global change. *Paleobiology*, 22; 152-176.

Panno, S.V., Curry B.B., Wang H., Hackley K.C., Liu C., Lundstorm C., and Zhou J., 2004. Climate change in southern Illinois, USA, based on the age and $\delta^{13}C$ of organic matter in cave sediments. *Quaternary Research*, 61; 301-313.

Pape, J.R., Banner, J.L., Mack, L.E., Musgrove, M., Guilfoyle, A., 2010. Controls on oxygen isotope variability in precipitation and cave drip water, central Texas, U.S.A.. *Journal of Hydrology*, 385; 203-215, doi: 10.1016/j.jhydrol.2010.02.021.

Peterson, L.C., Haug, G.H., Murray, R.W., Yarincik, K.M., King, J.W., Bralower, T.J., Kameo, K. , Rutherford, S.D., Pearce, R.B., 2000. Late Quaternary stratigraphy and sedimentation at ODP Site 1002, Cariaco Basin (Venezuela). *In*: Leckie, R.M., Sigurdsson, H. Acton, G.D., Draper, G. (Eds.), *Proc. ODP*, *Scientific Results*, 165: College Station, TX (Ocean Drilling Program); 85-99.

Peterson, L.C., Haug, G.H., 2006. Variability in the mean latitude of the Atlantic Intertropical Convergence Zone as recorded by riverine input of sediments to the Cariaco Basin (Venezuela). *Paleogeography, Paleoclimatology, Paleoecology*, 234; 97-113.

Pisias, N.G., Moore, T.C., 1981. The evolution of Pleistocene climate: a time series approach. *Earth and Planetary Science Letters*, 52; 450-458.

Poore, R.Z., Dowsett, H.J., Verardo, S., Quinn, T.M., 2003. Millennial- to century-scale variability in Gulf of Mexico Holocene climate records. *Paleoceanography,* 18(2); 1048, doi:10.1029/2002PA000868.

Porter, S.C., An, Z.S., 1995. Correlation between climate events in the North Atlantic and China during the last glaciation. *Nature*, 375; 305-308.

Raymo, M.E., 1997. The timing of major climate terminations. *Paleooceanography*, 12; 577-585.

Richards, D., Dorale, J., 2003. Uranium chronology and environmental applications of speleothems. *Rev. Mineral*., 52; 407–460.

Ridgewell, A.J., Watson, A.J., Raymo, M.E., 1999. Is the spectral signature of the 100 kyr cycle consistent with a Milankovitch origin? *Paleooceanography*, 14(4); 437-440.

Rozanski, K., Araguds-Araguds, L., Gonfiantini, R., 1992. Relation between long-term trends of 180 isotope composition of precipitation and climate. *Science*, 258; 981-985.

Scholz, D., Hoffmann, D., 2008. 230Th/U-dating of fossil reef corals and speleothems. *Quaternary Science*. 57; 52–77.

Seager, R., 2007. The turn of the century North American drought: Global context, dynamics, and past analogs, *J. Clim*., 20; 5527 – 5552, doi:10.1175/2007JCLI1529.1.

Severinghaus, J.P., Sowers, T., Brook, E.J., Alley, R.B., Bender, M.L., 1998. Timing of abrupt climate change at the end of the Younger Dryas interval from thermally fractionated gases in polar ice. *Nature*, 391; 141-146.

Shackelton, N.J., Opdyke, N.D., 1973. Oxygen isotope and paleomagnetic stratigraphy of equatorial Pacific care V28-238: oxygen isotope temperatures and ice volumes on a 10^5 year and 10^6 year scale. *Quaternary Research*, 3; 39-55.

Shen, C.C., Edwards, R.L., Cheng, H., Dorale, J.A>, Thomas, R.B., Moran, S.B., Weinstein, S.E., Edmonds, H.N., 2002. Uranium and thorium isotopic and concentration measurements by magnetic sector inductively coupled plasma mass spectrometry. *Chemical Geology*, 185 (3-4); 165-178.

Shurbaji, A.M., Phillips, F.M., 1995. A numerical model for the movement of H_2O, $H_2{}^{18}O$, and ^2HHO in the unsaturated zone. *Journal of Hydrology*, 171; 125-142.

Siegenthaler, U., Stocker, T.F., Monnin, E., Luthi, D., Schwander, J., Stauffer, B., Raynaud, D., Barnola, J., Fischer, H., Masson-Delmotter, V., Jouzel, J., 2005. Stable carbon cycle-climate relationship during the Late Pleistocene. *Science*, 310; 1313-1317.

Sowers, T., Bender, M., 1995. Climate records covering the last deglaciation. *Science*, 269 (5221), 210-214.

Springer, G.S., 2002: Stream processes in cave and surface stream flowing over limestone. West Virginia Speleological Survey Monograph, 3; 1-109.

Springer, G.S., Wohl, E.E., 2002. Empirical and theoretical investigations of sculpted forms in Buckeye Creek Cave, West Virginia. *Journal of Geology*, 110; 469-481.

Springer, G.S., Wohl, E.E., Foster, J.A., Boyer, D.G., 2003. Testing for reach-scale adjustments of hydraulic variables to soluble and insoluble strata: Buckeye Creek and Greenbrier River, West Virginia. *Geomorpgology*, 56; 201-217.

Springer, G.S., Rowe, H.D., Hardt, B., Edwards, R.L., Cheng, H., 2008. Solar forcing of Holocene droughts in a stalagmite record from West Virginia in east-central North America. *Geophysical Research Letters*, 35; doi:10.1029/2008GL034971.

Springer, G.S., Rowe, H.D., Hardt, B., Cocina, F.G., Edwards, R.L., Cheng, H., 2009. Climate driven changes in river channel morphology and base level during the Holocene and

Late Pleistocene of southwestern West Virginia. *Journal of Cave and Karst Studies*, 71(2); 121-129.

Steig, E.J., Grootes, P.M., Stuiver, M., 1994. Seasonal precipitation timing and ice-core records. *Science*, 266; 1885-1886.

Stein, M., Wasserburg, G.J., Aharon, P., Chen, J.H., Zhu, Z.R., Bloom A., Chappell, J., 1993. TIMS U-series dating and stable isotopes of the last interglacial event in Papua New Guinea. *Geochimica et Cosmochimica Acta,* 53; 2541–54.

Stuiver, M., Grootes, P.M., Braziunas, T.F., 1995. The GISP2 ^{18}O climate record of the past 16,500 years and the role of the sun, ocean and volcanoes. *Quaternary Research*, 44; 341-354.

Thompson, L.G., Davis, M.E., Mosley-Thompson, E., Sowers, T.A., Henderson, K.A., Zagorodnov, V.S., Lin, P.N., Mikhalenko, V.N., Campen, R.K., Bolzan, J.F., Francou, B., Cole-Dai, J., 1998. A 25,000 year tropical climate history from Bolivian ice cores. *Science*, 282; 1858-1864.

Udisti, R., Becagli, S., Castellano, E., Delmonte, B., Jouzel, J., Petit, J.R., Schwander, J., Stenni, B., Wolff, E.W., 2004. Stratigraphic correlations between the European Project for Ice Coring in Antartica (EPICA) Dome C and Vostok ice cores showing the relative variations of know accumulation over the past 45 kyr. *Journal of Geophysical Research*, 109(D8), doi:10.1029/2003JD004180.

Van Beynen, P., Febbroriello, P., 2006. Seasonal isotopic variability of precipitation and cave drip water at Indian Oven Cave, New York. *Hydrol. Process*. 20; 1793–1803.

Wackerbath, A., Scholtz, D., Fohlmeister, J., Mandini, A., 2010. Modeling the δ18O value of cave drip water and speleothem calcite. *Earth and Planetary Science Letters*, 299; 387-397.

Wang, Y.J., Cheng, H., Edwards, R.L., An, Z.S., Wu, J.Y., Shen, C.-C., Dorale, J.A., 2001. A high-resolution absolute-dated Late Pleistocene monsoon record from Hulu Cave, China. *Science,* 294; 2345–2348.

Wang, Y., Cheng, H., Edwards, R.L., He, Y., Kong, X., An, Z., Wu, J., Kelly, M.J., Dykoski, S.A., Li, X., 2005. The Holocene Asian Monsoon: Links to solar changes and North Atlantic Climate. *Science*, 308(5723); 854-857.

White, W.B., 2004. Palaeoclimate records from speleothems in limestone caves. In: Sasowsky, I.D., Mylroie, J. (Eds.), Studies of Cave Sediments. Physical and Chemical Records of Palaeoclimate. Kluwer Academic, New York, pp. 135– 175.

Williams, D.F., Thunell, R.C., Tappa, E., Rio, D., Raffi, I., 1988. Chronology of the Pleostocene oxygen isotope record: 0-1.88 m.y. B.P.. *Paleogeography, Paleoclimatology, Paleoecology,* 64; 221-240.

Williams, J.W., Post, D.M., Cwynar, L.C., Lotter, A.F., Levesque, A.J., 2002. Rapid and widespread vegetation responses to past climate change in the North Atlantic region. *Geology*, 30(11); 971-974.

Williams, P.W., 2008. The role of epikarst in karst and cave hydrology: a review. *International Journal of Speleology*, 3(1); 1-10.

Wilson, A.T., 1980. Isotope evidence for past climatic and environmental change. *Journal of Interdisciplinary History*, 10(4); 795-812.

Winograd, I.J., Coplen T.B., Landwehr, J.M., Riggs, A.C., Ludwig,K.R., Szabo, B.J., Kolesar, P.T., Revesz, K.M., 1992. Continuous 500,000-year climate record from vein calcite in Devils Hole. Nevada: *Science*, 258(5080); 255-260, doi: 10.1126/science.258.5080.255.

Winograd, I.J., Landwehr, J.M., Ludwig, K.R., Coplen, T.B., Riggs, A.C., 1997. Duration and structure of the past four interglaciations. *Quaternary Research*, 48(2); 141-154, doi: 10.1006/qres.1997.1918

Wright, J.D., 2000. Global climate change in marine stable isotope records, in Quaternary Geochronology: Methods and Applications to Paleoseismology. AGU Reference Shelf Series, Volume 4; Noller, J.S., J.M. Sowers, and W.R. Lettis, eds., p. 427-433.

Wynn, T.C., Read, J.F., 2006. Sequence-stratigraphic analysis using well cuttings, Mississippian Greenbrier Group, West Virginia. *AAPG Bulletin*, 90(12); 1869-1882.

Yuan, D., Cheng, H., Edwards, L., Dykoski, C.A., Kelly, M. J., Zhang, M., Qing, J., Lin, Y., Wang, Y., Wu, J., Dorale, J.A., An, Z., Cai, Y., 2004. Timing, duration, and transitions of the Last Interglacial Asian Monsoon. *Science*, 304(5670); 575-578.

Ziegler, M., Nurnberg, D., Karas, C., Riedemann, R., Lourend, L.J., 2008. Persistent summer expansion of the Atlantic Warm Pool during glacial abrupt cold events. *Nature Geoscience*; doi: 10.1038/ngeo277

BIOGRAPHICAL INFORMATION

Ashley Rachelle Wright graduated with her B.S. in Geology from the University of Texas at Arlington in August, 2008. Ashley Wright will receive her M.S. in Geology in December, 2011 and is currently employed as a geologist in the petroleum industry. Ashley graduates a member of Sigma Gamma Epsilon Earth Science Honor Society, American Association of Petroleum Geologists, Geological Society of America, and a sister of Alpha Phi International Fraternity. Although ecstatic to close this chapter in her life, Ashley plans to someday return to academia in pursuit of a Ph.D. in Geology.